

University of Louisville

## ThinkIR: The University of Louisville's Institutional Repository

---

Electronic Theses and Dissertations

---

8-2019

### Fluid flow analysis of diluted evaporating American whiskey droplets.

Martin J. Brown VI  
*University of Louisville*

Follow this and additional works at: <https://ir.library.louisville.edu/etd>



Part of the [Complex Fluids Commons](#), and the [Other Mechanical Engineering Commons](#)

---

#### Recommended Citation

Brown, Martin J. VI, "Fluid flow analysis of diluted evaporating American whiskey droplets." (2019). *Electronic Theses and Dissertations*. Paper 3249.  
<https://doi.org/10.18297/etd/3249>

This Master's Thesis is brought to you for free and open access by ThinkIR: The University of Louisville's Institutional Repository. It has been accepted for inclusion in Electronic Theses and Dissertations by an authorized administrator of ThinkIR: The University of Louisville's Institutional Repository. This title appears here courtesy of the author, who has retained all other copyrights. For more information, please contact [thinkir@louisville.edu](mailto:thinkir@louisville.edu).

FLUID FLOW ANALYSIS OF DILUTED EVAPORATING AMERICAN WHISKEY  
DROPLETS

By

Martin Joseph Brown VI

B.S. Mechanical Engineering, University of Louisville, 2018

A Thesis  
Submitted to the Faculty of the  
University of Louisville  
J. B. Speed School of Engineering  
as Partial Fulfillment of the Requirements  
for the Professional Degree

MASTER OF ENGINEERING

Department of Mechanical Engineering

August 2019



Fluid flow analysis of diluted evaporating American whiskey droplets.

Submitted by:

---

Martin Joseph Brown VI

A Thesis Approved On

---

(Date)

By the Following Reading and Examination Committee

---

Dr. Stuart J. Williams, Thesis Director

---

Dr. Gerold Willing

---

Dr. Ellen Brehob

## ACKNOWLEDGMENTS

I would like to thank a great number of people for their assistance in my journey to finishing my master's degree and especially my thesis. First, I would like to thank my parents, Marty and Amy Brown, for their support and encouragement these past 5 years in college as well as in my entire life. A special thanks to my father and grandpa, Martin Brown V & IV, respectively, for nurturing my love of math and engineering growing up.

Secondly, I would like to thank Dr. Williams for the numerous hours he has dedicated assisting me in the lab and listening to all of my ideas no matter how abstract they may be. I have had the good fortune to meet your family and I can say without a doubt that your ability as a professor and mentor is only surpassed by the quality of person you are with your family.

Finally, I would like to thank Adam Carrithers, whom I have worked closely with on writing and preparing the material for "Multiscale self-assembly of unique web-like structures from evaporated drops of dilute American whiskeys", for his time, help and friendship these past 12 months. In addition, I would like to thank Mohamed "Mido" Rashed and Md Mahmudur "Rony" Rahman for their time answering the multitude of questions I had about various technical issues that arose.

## ABSTRACT

The recent discovery of the unique structures, whiskey webs, formed when the evaporation of diluted American whiskey, has raised many questions as to the nature of the structures. Their formation process follows as such: (1) dilution of the whiskey to form nanoaggregates, (2) formation of a monolayer at the air-liquid interface, (3) chaotic ethanol evaporation caused monolayer collapse (via dynamic pressure), (4) bulk fluid evaporation caused monolayer collapse (via reduction of surface area), where the web-like structures reside on the surface, and finally, (5) web-like structures deposit on the substrate. The webs imaged via SEM had a striking resemblance to the “twisted ribbon fold” found in literature. There has been significant research within monolayer collapse where various mechanisms have been found which describe how they collapse; this work focused on the role of ethanol evaporation of sessile droplets in the formation of whiskey webs. The study will identify how characteristics (maturation, proof, surfactants, filtrations, congeners, and whiskey web patterns) influence the fluid velocity to the greatest degree. Since the ethanol evaporation is believed to be the largest contributor to the web-like structure formation process, it was studied here. This work will help to understand the role the ethanol evaporation has to the uniqueness of the web structures. These findings contribute towards correlating monolayer collapse mechanisms and feature characteristics to the intrinsic properties within American whiskey.

## TABLE OF CONTENTS

ACKNOWLEDGMENTS .....	i
ABSTRACT.....	ii
LIST OF TABLES .....	v
LIST OF FIGURES .....	vi
I. INTRODUCTION.....	1
A What is self-assembly and why it's important? .....	1
B. WHAT'S A COLLOID? .....	2
C. COLLOID SELF-ASSEMBLY METHODS.....	3
1. EVAPORATIVE METHODS .....	4
D. COLLAPSE MECHANISMS OF MONOLAYERS.....	10
E. BOURBON BACKGROUND .....	12
F. WHISKEY WEBS.....	13
G. MOTIVATION .....	15
II. Materials and Methods.....	18
A. Background on PIV.....	18
B. EXPERIMENTAL DESCRIPTION .....	21
C. SAMPLE PREPARATION.....	23
1. All Experiments (1-6) .....	23
2. SURFACTANT EXPERIMENT (3) .....	25
3. FILTRATION EXPERIMENT (4).....	27
D. EXPERIMENTAL SET-UP .....	27
E. FRAME ANALYSIS.....	35
III. RESULTS AND DISCUSISON .....	41
A. DISTILLATION AND MATURATION EXPERIMENT (1).....	41
B. PROOF EXPERIMENT (2).....	42
C. SURFACTANT EXPERIMENT (3).....	43
D. FILTRATION EXPERIMENT (4) .....	45
E. CONGENERS EXPERIMENT (5) .....	46
1. REPEATABILITY EXPERIEMENT.....	50

IV. CONCLUSION.....	52
V. RECOMMENDATIONS.....	56
VI. APPENDICES .....	59
VII. LIST OF REFERENCES .....	64
VIII. VITA .....	69



## LIST OF TABLES

Table I - Description of colloidal solutions.....	3
Table II - Seed Concentration Dilution Table.....	25
Table III - High Speed camera settings.....	31
Table IV - External Trigger Specifications .....	33
Table V – Summarized Results.....	55

## LIST OF FIGURES

<p>Figure 1 - Modal of the three stages of evaporation in a binary solution (1) first stage where the volatile (ethanol) evaporates and the CCR model is followed (2) transitional stage where the contact line de-pins and the contact angle increases to an angle similar to a pure bulk fluid ( water) droplet (3) the bulk fluid (water) contact angle, height, base all decrease at the same rate. (Sefiane, Tadrist et al. 2003).....</p> <p>Figure 2 - American whiskey exhibiting the coffee-ring effect. The white arrows are pointing to the contact line where the majority of the particles are deposited on the substrate. ....</p> <p>Figure 3 - Schematic of the competing Marongoni flows after the ethanol has evaporated within the droplet. Figure reproduced from (Kim, Boulogne et al. 2016).....</p> <p>Figure 4 - Model showing how the absorbed polymer adheres to the substrate and then provides a rough and dense structure to capture particles as the contact recedes to the center of the droplet. Figure reproduced from (Kim, Boulogne et al. 2016).....</p> <p>Figure 5 - Twisted-Ribbon fold found in literature, the scale bar is 1 <math>\mu\text{m}</math>. Figure reproduced from (Ries and Swift 1987).....</p> <p>Figure 6 - Whiskey webs Whiskey web patterns, approximately 2 mm in diameter, formed by various off-the-shelf whiskey products diluted to 20-25% alcohol by volume: (a) Old Rip Van Winkle 10 Year<sup>TM</sup>, (b) Four Roses Single Barrel<sup>TM</sup>, (c) Baker’s Bourbon<sup>TM</sup>, (d) Van Winkle Special Reserve 12 Year<sup>TM</sup>, (e) O.K.I. 8 Year<sup>TM</sup>, (f) Woodford Reserve Double Oaked<sup>TM</sup>, (g) Pappy Van Winkle 15 Year<sup>TM</sup>, (h) Jack Daniel’s Single Barrel<sup>TM</sup>, (i) I.W. Harper 15 Year<sup>TM</sup>, (j) Pappy Van Winkle 20 Year<sup>TM</sup>, (k) 1792 Small Batch<sup>TM</sup>, (l) Jim Beam Single Barrel<sup>TM</sup>, (m) Pappy Van Winkle 23 Year<sup>TM</sup>, (n) Heaven Hill 6 Year Bottled in Bond<sup>TM</sup>, (o) Maker’s Mark Cask Strength<sup>TM</sup>. This figure was reproduced from (Brown &amp; Carrithers 2019 submitted).....</p> <p>Figure 7: SEM images of Whiskey web, sample is of Woodford Reserve Double Oaked. Figure reproduced from (Brown &amp; Carrithers 2019 submitted).....</p> <p>Figure 8 - Whiskey webs a) Maker’s Mark Cask Strength b) 1792 Small batch c) Jim Beam Single Barrel. The web patterns shown appear different in nature, this observation has been validated by numerous qualitative experiments. Figure reproduced from (Brown &amp; Carrithers 2019 submitted). ....</p> <p>Figure 9 - PIV window based cross correlation. Two successive images regions are compared via cross correlation function to determine the resulting vector. Figure reproduced from (Choi, Kim et al. 2011) .....</p> <p>Figure 10 - PIV settings for PIVlab’s displaying interrogation area and step size in addition to multiple passes (Thielicke 2014). ....</p> <p>Figure 11 - PIV interrogation window with a 50% step size. Figure reproduced from (Thielicke 2014).....</p> <p>Figure 12- Overall Figure of the Mechanical Set-up a) Wave-form generator b) High-Speed camera c)LED ring light attaches and height can be adjusted d) platform where the slide sits above the lens e) base of the microscope where the 1.5X adjustment knob is located f)DC power supply for the LED ring light g) temperature and humidity sensor. 28</p>	<p>6</p> <p>7</p> <p>9</p> <p>10</p> <p>11</p> <p>14</p> <p>15</p> <p>16</p> <p>19</p> <p>20</p> <p>20</p> <p>28</p>
--	--

Figure 13 - DC power supply used for the ring light attachment. ....	29
Figure 14 - White Teflon masked microscope slides.....	29
Figure 15 - Image taken by the mono colored high-speed camera. Notice the halo around the edge of the droplet. Steps were taken to attempt to minimize the thickness of halo but could not be eliminated. ....	30
Figure 16 - Black printed PTFE mask which had poor quality, not used in study. ....	30
Figure 17 - Keithley 3390 50 MHz Arbitrary waveform generator used to trigger the high speed camera into taking the right amount of pictures. ....	32
Figure 18: HiSpec Manual (Page 85) and actual image of wires connecting the waveform generator to the high-speed camera. ....	33
Figure 19 – Signal Diagram showing how the square wave is used to control the number of images captured. ....	34
Figure 20 - An arbitrary line is drawn within the droplet. Any distance line can be used because of the formula below. ....	36
Figure 21 - Example of a masked and processed image pair is represented within PIVlab. ....	37
Figure 22: a) Velocity magnitude and b) vorticity images exported from PIVlabs.....	38
Figure 23. Vorticity (a) and Velocity Magnitude (b) data from the Distillation and Maturation experiment. Notice the trends between the two figures are almost identical to each other. ....	40
Figure 24: Distillation and maturation results. ....	41
Figure 25 - Top 20% vectors for varied dilution of an American whiskey .....	42
Figure 26: The magnitude of velocity of samples prepared with varied levels of SDS. ..	44
Figure 27 - Velocity Magnitude of solutions after various method of filtration as well as a control. ....	45
Figure 28 - Velocity Magnitude of an unfiltered American whiskey and one that is held at the same ABV while diluting the congeners present in the solution. ....	47
Figure 29 - Velocity Magnitude of two distinctly different web-like structures that make up two distinctly different whiskey web patterns. ....	49
Figure 30 - Repeatability test 25% ABV Buffalo Trace. All three sample are consistent within the magnitude and duration of chaotic flow. ....	50
Figure 31 - Schematic showing the vortices are 3D not just 2D. Figure reproduced from (Bennacer and Sefiane 2014). ....	51
Figure 32: Experiment 1. Top 20% velocity magnitude versus time .....	62
Figure 33: Experiment 1. Top 10% velocity magnitude versus time .....	62
Figure 34: Experiment 1. Top 5% velocity magnitude versus time .....	63

## I. INTRODUCTION

### A What is self-assembly and why it's important?

The building blocks of life and structures on the molecular and atomic level are not built by someone in a lab. Instead they are generally formed by a self-assembly process. A definition of self-assembly is

“the process in which a system’s components—be it molecules, polymers, colloids, or macroscopic particles—organize into ordered and/or functional structures or patterns as a consequence of specific, local interactions among the components themselves, without external direction.” (Varga 2016)

There are many commonly known structured patterns that are found in nature like that of the honeycomb among others (Rey, Yu et al. 2018). There is a lot of research around carbon nanotube self-assembly for semi-conductor silicon technology (Fan, Chapline et al. 1999) and gold nanowire production (Fullam, Cottell et al. 2000). The ability to have

particles self-assemble repeatably while also using minimal energy and relatively low fabrication time is an interest of scientists and engineers (Masuda, Itoh et al. 2005). This could lead to further control of microfabrication of devices and sensors. In addition to the electrical nanofabrication implications, self-assembly is of interest for the biological community due to the self-assembly of DNA and proteins (Varga 2016) and biological nanostructured biomaterials through self-assembly of peptides and proteins (Zhang, Marini et al. 2002).

### B. WHAT'S A COLLOID?

Colloids are an important part of people's daily lives and for the most part they go unnoticed. A colloid can be defined as a particle that has a linear dimension between 1  $\mu\text{m}$  and 1 nm (Hiemenz and Rajagopalan 1997). This definition is the very basic of such and can be expanded into many subject matters. Colloidal systems can be further classified by what is the continuous phase and what the dispersed phase. There are many examples of such and can be seen in Table I.

Table I

Descriptive names and classification of colloidal solutions. This table was reproduced from (Hiemenz and Rajagopalan 1997).

<b>Continuous phase</b>	<b>Dispersed phase</b>	<b>Descriptive names</b>
Gas	Liquid	Fog, mist, aerosol
Gas	Solid	Smoke, aerosol
Liquid	Gas	Foam
Liquid	Liquid	Emulsion
Liquid	Solid	Sol, colloidal solution, gel, suspension
Solid	Gas	Solid foam
Solid	Liquid	Gel, solid emulsion
Solid	Solid	Alloy

The area of interest this study was concerned with was an emulsion, liquid-liquid. Within this category, they can then be broken up into how the dispersed colloidal particles react to the medium. The terms lyophobic and lyophilic refer to the cases where the particles are “solvent fearing” and “solvent loving”, and when the medium is composed of water the terms are then hydrophobic and hydrophilic, “water fearing” and “water loving” (Hiemenz and Rajagopalan 1997).

### C. COLLOID SELF-ASSEMBLY METHODS

There are two main types of self-assembly methods, static and dynamic. Static self-assembly methods do not dissipate energy, however may require an input of energy (stirring) but once formed the system is stable (Whitesides and Grzybowski 2002, Xu,

Wang et al. 2016). Dynamic self-assembly is more complex as they only occur if the system is dissipating energy.

Typical static self-assembly methods include spin coating, physical coating, electromagnetic, noncovalent, interface and evaporation induced self-assembly (Xu, Wang et al. 2016). Spin coating self-assembly takes advantage of centrifugal forces after depositing a colloidal suspension onto a clean substrate. The quality and thickness of the resulting crystalline structure is controlled by the rotation speed, concentration of colloidal suspension and the wettability of the substrate (Xu, Wang et al. 2016). Studies have developed different spin speeds and accelerations to achieve controlled coverage area (Cheng, Jönsson et al. 2014), and the use of a different solvent to produce a higher yield coverage area as well as close-packed monolayer with good uniformity (Choi, L Alford et al. 2014). This process is often paired with another process like interface and physical template self-assembly (Xu, Wang et al. 2016). In this study, the focus was on evaporative and interfacial static self-assembly.

## 1. EVAPORATIVE METHODS

The basic method of evaporative self-assembly involves placing a concentrated colloidal suspension onto a substrate or inserting the substrate in the suspension solution (Xu, Wang et al. 2016). Environmental conditions such as humidity, temperature, and pressure need to be controlled so the colloidal particles will self-assemble into the desired 2D or 3D structure. The structure will self-assemble under the influence of factors like surface tension, capillary forces, and thermal migration (Xu, Wang et al. 2016). Various orientations of the substrate for which the colloidal monolayers form have been studied,

horizontal (Micheletto, Fukuda et al. 1995), vertical (Kim, Im et al. 2005) and sloped (Wu, Zhang et al. 2013). Also various solvents evaporation rate effects have been analyzed for their impact on the monolayer composition quality (Burmeister, Badowsky et al. 1999, Park and Moon 2006).

Interfacial self-assembly revolves around the idea that particles will align themselves at the phase boundary, air-liquid, liquid-liquid (Isa, Kumar et al. 2010), and liquid-solid interface (Blodgett 1935). Interfacial self-assembly was the earliest proposed method to produce 2D and 3D colloidal structures, and in the 1930's Langmuir and Blodgett succeeded in transferring an amphipathic monolayer from a liquid air interface to a substrate (Blodgett 1935, Blodgett and Langmuir 1937). Additional researchers have created 2D monolayers at the air-liquid interface with the help of a surfactant based solution for nanofabrication (Li, Hong et al. 2009).

a. SESSILE DROPLET EVAPORATION. Sessile droplet evaporation is at the center of processes that involves inkjet printing (Kawase, Siringhaus et al. 2001), painting, controlled cooling of integrated circuits (Shedd and Pautsch 2005). Sessile as defined by Merriam-Webster, means attached directly by the base. A sessile droplet is composed of a single droplet of solution placed on a substrate. The sessile droplet technique is used mainly to measure surface energies of the substrate or solution where the other is known. There are two main evaporation methods for a sessile droplet, constant contact angle (CCA) and constant contact radius (CCR) (Picknett and Bexon 1977). All sessile droplets will behave like one or the other, or a combination of both. In a homogenous solution the evaporation laws are straightforward, however it becomes very complicated when the solution is a mixture, suspension or both (Liu, Bonaccorso et al. 2008)



a (i). ALCOHOL/WATER EVAPORATION The evaporation process of the binary mixture of ethanol and water has been of interest in the science community. After analysis it was determined that there were three stages of evaporation (Sefiane, Tadrist et al. 2003).

This was supported by the similarity of the evaporation rates between the first stage of the binary solutions and pure ethanol. Subsequently the evaporation rate of the third stage of the binary solutions and pure water were comparable. The second stage was the transitional stage where any remaining ethanol was evaporated, and the evaporation rate was not linear. The evaporation rate is affected by the contact angle between the droplet and the substrate (Sefiane, Tadrist et al. 2003). There was a dynamic change of its contact angle based on surface tension of the droplet. With that in mind, the hydrophobicity of the substrate can change the contact angle and was needed to be considered in the experiment.

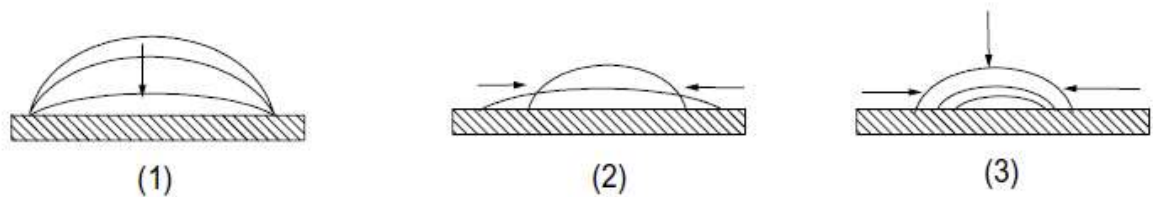


Figure 1 - Modal of the three stages of evaporation in a binary solution (1) first stage where the volatile (ethanol) evaporates and the CCR model is followed (2) transitional stage where the contact line de-pins and the contact angle increases to an angle similar to a pure bulk fluid ( water) droplet (3) the bulk fluid (water) contact angle, height, base all decrease at the same rate. (Sefiane, Tadrist et al. 2003)

To understand the mechanisms governing the three stages seeded particles were added to the fluid and observed. They found that multiple vortices were present in the first stage of evaporation (Christy, Hamamoto et al. 2011, Bennacer and Sefiane 2014). This is followed by the transitional stage where the vortices dissipate and transition to a relatively

calm radially fluid flow characterizing the third stage (Christy, Hamamoto et al. 2011, Bennacer and Sefiane 2014).

b. COFFEE-RING EFFECT. The coffee-ring effect is a phenomenon that has long been of interest in the fluid dynamic community, in which particles are concentrated at the droplets outer edge. The phenomenon gets its name due to coffee spills producing the patterns described. It has been found that this occurs due to capillary flow (Deegan, Bakajin et al. 1997). As the solution evaporates from the edge of the droplet fluid travels from the center of the droplet out to the edge replacing the loss of fluid (Deegan, Bakajin et al. 1997).

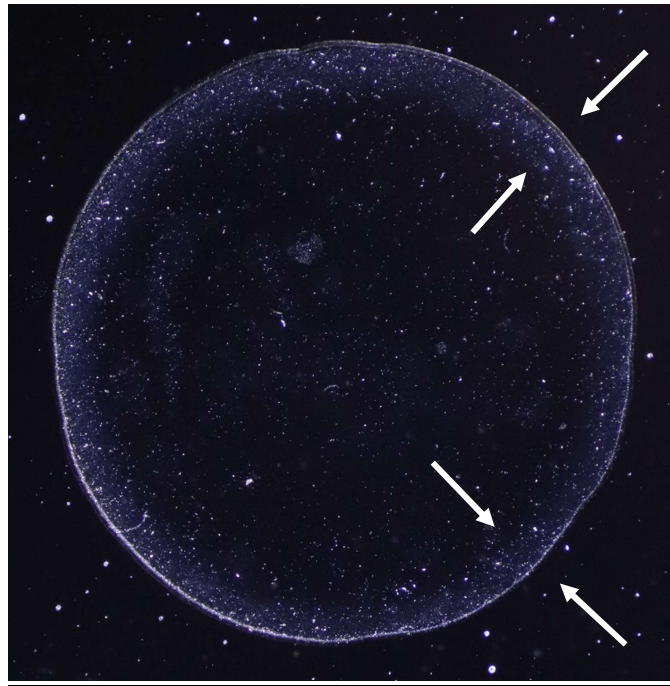


Figure 2 - American whiskey exhibiting the coffee-ring effect. The white arrows are pointing to the contact line where the majority of the particles are deposited on the substrate.

b (i). MODIFICATION OF THE COFFEE-RING EFFECT. The coffee-ring effect has always been an interesting subject of research for scientists; however, the deposition pattern of a thin film is most desired. Many scientists are actively working on how to suppress this phenomenon. There are three methods to suppress the coffee ring; de-pinning of the contact line, disturbing the capillary flow, and/or trapping the solute. To suppress the coffee-ring effect various techniques have been utilized: changing the hydrophobicity of the substrate relative to the droplet, electrowetting, and manipulating the Marangoni flow through both surfactant and thermal manipulation, changing the geometry of the particles deposited on the substrate, and changing the droplet geometry. (Mampallil and Eral 2018).

In this work, disrupting capillary flow will be explored further. The thermal conductivity ratio between the liquid sessile droplet and substrate in addition to the contact angle dictates the direction of the thermal Marangoni flows (Ristenpart, Kim et al. 2007). However thermal Marangoni flows can be suppressed by a small concentration of surfactants (Hu and Larson 2005). Surfactants dominate fluid flow in a system which produces strong radially inward flow where particles concentrate at the center of the droplet. Other materials including surfactant like polymers have also been studied to suppress the coffee-ring affect (Seo, Jang et al. 2017).

b(ii). STONE'S WORK A group out of Princeton was interested in understanding why scotch whiskey (Glenlivet 12 year) resulted in a thin film after the evaporation of a sessile droplet. In their experiments they placed a 0.60  $\mu\text{L}$  droplet on a cleaned glass slide and let it evaporate at ambient conditions. They identified that there were three stages of the evaporative process, which is consistent with other binary ethanol/water based systems

(Christy, Hamamoto et al. 2011). It was also determined that during the stages of evaporation Marangoni flow was the driving force for fluid motion. They found that there were three contributors and that they could be ranked in hierarchical order as such 1) solutal, 2) surfactant and 3) thermal (Kim, Boulogne et al. 2016). The first stage is dominated by the ethanol evaporation which produces a solutal Marangoni affect due to the ethanol concentration gradient present. Vortices are produced during this stage and overshadow the two other competing forces. After this stage is complete the surfactant driven flow proceeds where flow is directed toward the center of the droplet opposite as described previously.

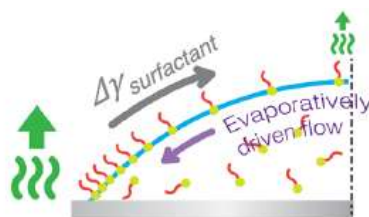


Figure 3 - Schematic of the competing Marangoni flows after the ethanol has evaporated within the droplet. Figure reproduced from (Kim, Boulogne et al. 2016)

They determined that the surfactant induced Marangoni flows were based on the natural surfactants derived from grains used in the mash. However, the surfactant alone does not explain the uniform particle deposition. The chemical composition of whiskey has been extensively studied and natural polymers have been identified. It was known that polyethylene oxide (PEO) can absorb onto silica creating a pseudo brush structure on glass slides (J. C. Braithwaite and F. Luckham 1997). This was shown to provide a rough surface for the particles to adhere to as the contact line recedes from the out edge of the droplet into the center as seen in Figure 4. Not until they added both a surfactant and a polymer to

a binary solution of ethanol and DI water were they able to artificially achieve some level of thin film deposition.

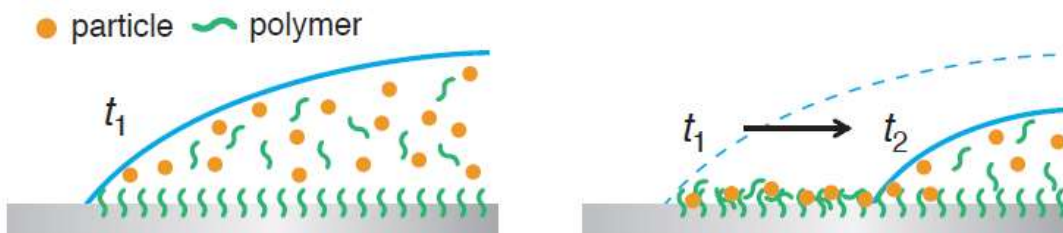


Figure 4 - Model showing how the absorbed polymer adheres to the substrate and then provides a rough and dense structure to capture particles as the contact recedes to the center of the droplet. Figure reproduced from (Kim, Boulogne et al. 2016).

#### D. COLLAPSE MECHANISMS OF MONOLAYERS

A monolayer is a single layer of atoms, molecules, or cells. Langmuir monolayers are one molecule thick layer of amphiphilic material on top of a liquid subphase (Kendall and Monroe 1917). They are formed by placing the material on the surface of the subphase where it spreads evenly across.

Monolayer testing is done in a Langmuir trough (Ybert, Lu et al. 2002, Ybert, Lu et al. 2002, Phan, Lee et al. 2016). A Langmuir trough is a thin basin that contains the sub-phase (water) and barriers at either end. The barriers slowly proceed inward reducing the surface area for the molecules to occupy. The compression rate is controlled, and as the surface area decreases the surface pressure increases and measurements are recorded. Monolayers will collapse when experiencing with a surface pressure greater than the equilibrium spreading pressure (Ybert, Lu et al. 2002).

There are three collapse mechanisms that are generally accepted: slow collapse, giant folds, multiple folds (Ybert, Lu et al. 2002, Ybert, Lu et al. 2002). The slow collapse occurs via nucleation of multilayer islands which occurs at low surface pressures. At high surface pressure two folding mechanisms occur one during low compression rates, giant folds, and the other at higher compression rates, multiple folds. The collapse pressure of  $72 \times 10^{-3} \frac{N}{m}$  was analytically calculated, however collapse pressures are less than that value. It was concluded that folds then will collapse or fold at impurities within the monolayer (Ybert, Lu et al. 2002).

A monolayer collapsed structure that was of interest in this study was called a twisted ribbon fold (Ries and Swift 1987). This structure was the result of a monolayer that collapsed buckling, folding, and breaking off to form a bilayer. This is confirmed because of the twisted nature of the structure, if it was still attached to the monolayer this would not be present, as seen in Figure 5.

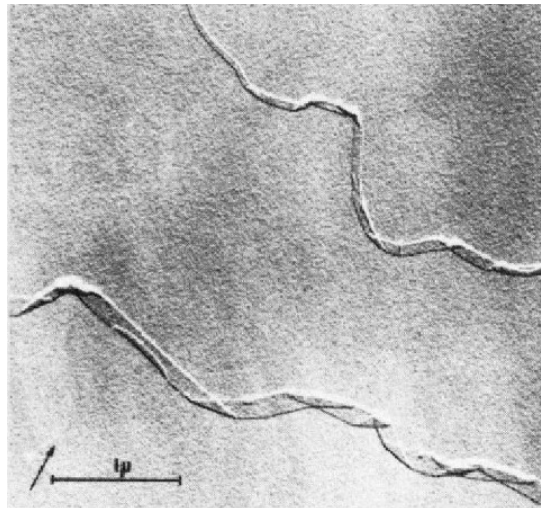


Figure 5 - Twisted-Ribbon fold found in literature, the scale bar is 1 μm. Figure reproduced from (Ries and Swift 1987).

## E. BOURBON BACKGROUND

The most popular spirit in the state of Kentucky is bourbon, in which there are more barrels currently in the state ,7.5 million, than there are people, 4.3 million. (Coomes 2019). The bourbon industry alone accounts for 8.6 billion dollars of economic output for the state of Kentucky (Coomes 2019).

Kentucky Bourbon is also considered an American whiskey. There are many other types of whiskeys (Irish whiskey, Canadian whiskey, Scotch whiskey, rye whiskey ..) each having their own constraints that have to be followed to be classified as such (Piggott, Sharp et al. 1989).

An American whiskey is a spirit distilled at an alcohol by volume (ABV) no greater than 95% from a distiller's "beer" or fermented mash (Pass and Lambart 2003). The mash is a combination of grains (corn, barely, rye, wheat) called a mash bill. After distillation, but before the maturation process, it is called distillate or more commonly "white dog". This "white dog" is then put into a new oak charred barrel and aged for at least two years, but more commonly four years or more.

During the fermentation process, constitutes known as congeners, are produced through side reactions and contribute to the smell and taste of the bourbon (Brown & Carrithers 2019 submitted). Surfactants are naturally derived from the grain in the form of phospholipids (Kim, Boulogne et al. 2016) while maturation increases the concentration of acids, esters, and dissolved solids (Crampton and Tolman 1908, Liebmann and Rosenblatt 1943). Many of these organic compounds are amphipathic and alcohol-soluble (Karlsson

and Friedman 2017) which when diluted align themselves at the air-liquid interface forming a monolayer.

## F. WHISKEY WEBS

The following description of whiskey web research is an abbreviated description from “Multiscale self-assembly of unique web-like structures from evaporated drops of dilute American whiskeys” by Brown & Carrithers et al. Refer to their manuscript for an expanded explanation of the current understanding of whiskey webs.

When a 1.0  $\mu\text{L}$  sessile droplet of diluted (20-25 % ABV) American whiskey is placed on a cleaned glass slide and evaporated, the deposited pattern left on the substrate is what is called a Whiskey web. At low ABV (< 15%) droplets exhibit the well know coffee-ring pattern and at higher ABV (> 35%) a thin film is formed. This phenomenon was unique to American whiskey, where 65 of 66 tested samples have formed webs. Non-American whiskey samples tested ( $n= 13$ ), Canadian, Irish, Scotch and white dog ( $n=5$ ), did not form webs. The distinguishing factor being that American whiskey is aged in a new charred oak barrel. Their findings strongly suggest that the larger concentration of water insoluble components derived during the maturation process are critical to the web formation process (Crampton and Tolman 1908). Another intriguing aspect of the whiskey webs is that they are qualitatively unique to each product, while being qualitatively repeatable between tests from the same sample (Figure 6).



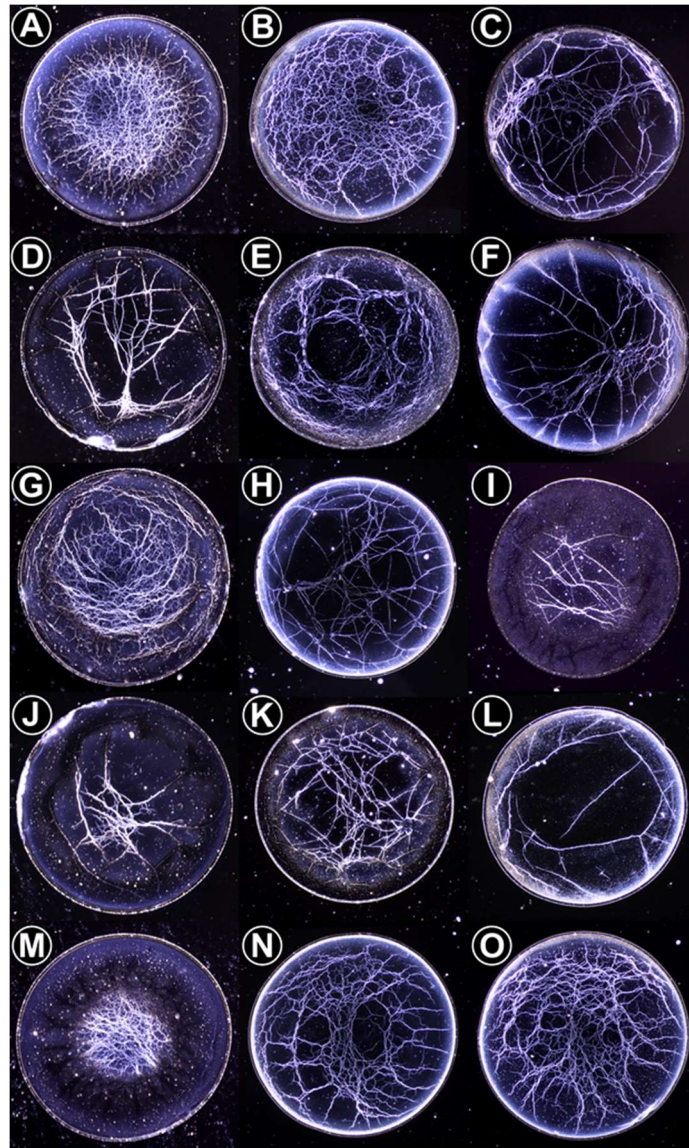


Figure 6 - Whiskey webs Whiskey web patterns, approximately 2 mm in diameter, formed by various off-the-shelf whiskey products diluted to 20-25% alcohol by volume: (a) Old Rip Van Winkle 10 Year<sup>TM</sup>, (b) Four Roses Single Barrel<sup>TM</sup>, (c) Baker's Bourbon<sup>TM</sup>, (d) Van Winkle Special Reserve 12 Year<sup>TM</sup>, (e) O.K.I. 8 Year<sup>TM</sup>, (f) Woodford Reserve Double Oaked<sup>TM</sup>, (g) Pappy Van Winkle 15 Year<sup>TM</sup>, (h) Jack Daniel's Single Barrel<sup>TM</sup>, (i) I.W. Harper 15 Year<sup>TM</sup>, (j) Pappy Van Winkle 20 Year<sup>TM</sup>, (k) 1792 Small Batch<sup>TM</sup>, (l) Jim Beam Single Barrel<sup>TM</sup>, (m) Pappy Van Winkle 23 Year<sup>TM</sup>, (n) Heaven Hill 6 Year Bottled in Bond<sup>TM</sup>, (o) Maker's Mark Cask Strength<sup>TM</sup>. This figure was reproduced from (Brown & Carrithers 2019 submitted).

When American whiskey is diluted, the molecules present are driven to the surface due to their hydrophobicity. These molecules form a monolayer at the air-liquid interface. Ethanol diffuses to the surface and evaporates first, creating multiple vortices. The evaporation stages follow that of both the binary solution (Sefiane, Tadrist et al. 2003) and scotch whiskey (Kim, Boulogne et al. 2016). The web-like structures that make up the whiskey webs form by monolayer collapse. This is supported by an SEM image that shows a twisted ribbon fold, shown in Figure 7.

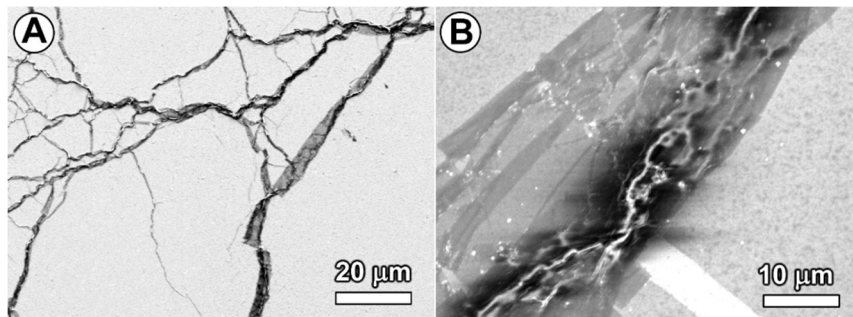


Figure 7: SEM images of Whiskey web, sample is of Woodford Reserve Double Oaked. Figure reproduced from (Brown & Carrithers 2019 submitted).

The work also shows that with the addition of various chemicals web structures change, suggesting that the chemical uniqueness between product contribute to the uniqueness of the web patterns.

## G. MOTIVATION

During this time, it is proposed that the ethanol evaporation induced vortices produce the stress needed to collapse the monolayer (Brown & Carrithers 2019 submitted). It is intriguing that whiskey web patterns seem to exhibit multiple different types of web structures while considering there are three types of monolayer collapse mechanisms.

Some are thin and “webby” (Figure 8a) where some are long thick strands (Figure 8c) as well as a web structure that is somewhere in between (Figure 8b).



Figure 8 - Whiskey webs a) Maker’s Mark Cask Strength b) 1792 Small batch c) Jim Beam Single Barrel. The web patterns shown appear different in nature, this observation has been validated by numerous qualitative experiments. Figure reproduced from (Brown & Carrithers 2019 submitted).

While this work still will not definitively conclude if certain webs structures are a result of the different collapse mechanisms it will explore the velocity magnitude and vorticity trends between samples tested.

Within the scope of this work, a process for flow visualization and characterization was established through PIV analysis. The process was used to gain insight into the fluid velocity of the evaporating droplets. The fluid velocity was used as a tool to compare the effects of variable manipulation (maturation, distillation, proof, surfactants, filtrations, congeners, and whiskey). Therefore, samples were chosen in the attempt to isolate a specific variable that has had some qualitative effect on the whiskey web pattern.

This study was important in quantifying the flow field within the droplet. Up to this point, there had been no analysis of the samples during the evaporation process. The ability

to compare the fluid velocity of samples and cross reference those findings to their web patterns helped to highlights the role evaporation had in the web formation process.

## II. Materials and Methods

### A. Background on PIV

Particle Image Velocimetry (PIV) is an analytical technique that measures a 2D velocity field. The process of PIV involves seeding a fluid with particles after which sequential images are taken and analyzed in pairs to determine fluid movement. It compares the particles from the first image to the second, determining the distance the particles travel and calculates a rate of fluid motion (Nguyen and Wereley 2010). PIV has been used across fields such as biomedical, aerospace and automotive for both micro and macroscale problems. (Raffel, Willert et al. 1998) Figure 8 shows the more in-depth window-based analysis technique for PIV.

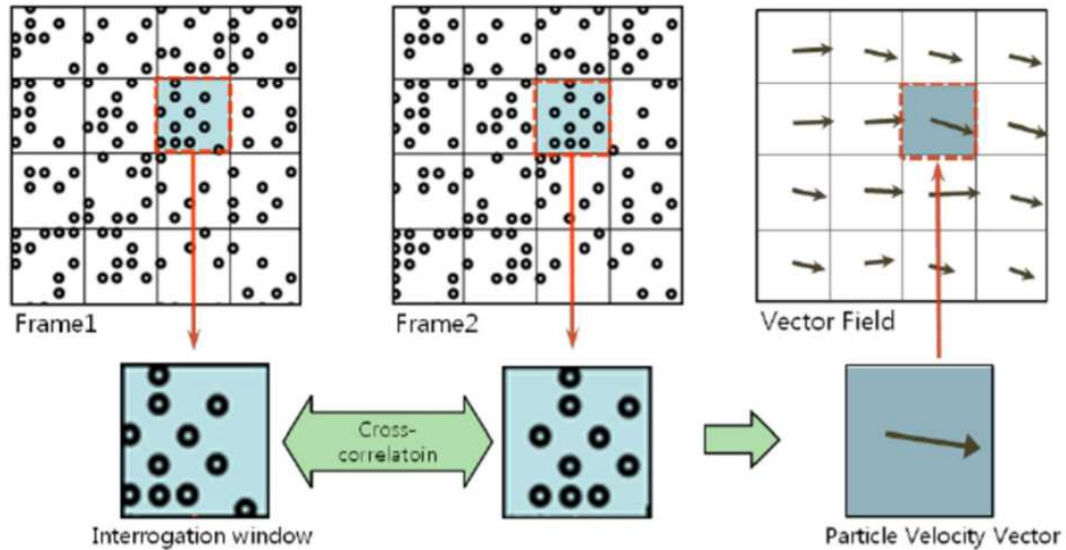


Figure 9 - PIV window based cross correlation. Two successive images regions are compared via cross correlation function to determine the resulting vector. Figure reproduced from (Choi, Kim et al. 2011)

More specifically Frame1 and Frame2 are broken up into regions called interrogation windows. The size of the windows can be controlled within the program. The particles seen in Frame1's window is statistically compared to the corresponding window in Frame2 and a resulting vector is calculated. The vectors are converted into a velocity when a reference distance is inputted into the program converting pixel size to actual distance and the time between frames is inserted from the calculated frame rate.

Terms that are addressed when discussing PIV are the number of passes that the program uses to calculate vectors, step size and interrogation area. The variable choices in PIVlab are shown in Figure 10.

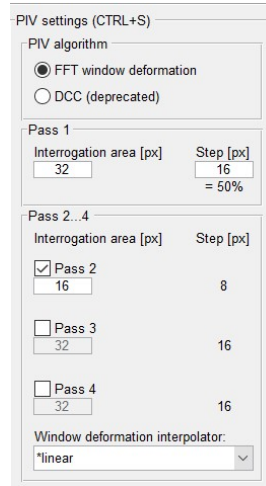


Figure 10 - PIV settings for PIVlab's displaying interrogation area and step size in addition to multiple passes (Thielicke 2014).

In Figure 9 each window is converted into one vector that is placed at its center. The 'step size' overlaps the windows such that a vector is calculated for the window size chosen then moves 50% of the window size in every direction and calculates it for that region as well. This produces nine vectors for each window which is shown in Figure 10.

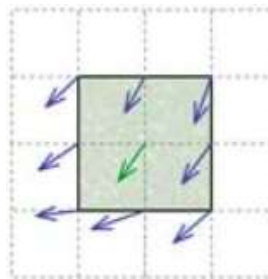


Figure 11 - PIV interrogation window with a 50% step size. Figure reproduced from (Thielicke 2014).

The larger the interrogation window the less accurate the resultant vector will be because, as seen in Figure 10 there is nonuniform flow. However, as the window size decreases the higher the concentration of the particles is needed to yield acceptable results.



Good PIV data is achieved when there are 10+ particles in the interrogation window. To advance the precision of the data the values calculated from the first pass are used as offsets for the second pass while at the same time the size of the window is reduced. So instead of comparing Frame1 to Frame2, it will compare Frame1 to Frame2 plus the offset determined by the first pass. Each subsequent pass is looking at the same pair of frames. PIVlab has the capability of performing four passes. Further characteristics can be derived from the velocity components, such as velocity magnitude, vorticity, divergence among others.

## B. EXPERIMENTAL DESCRIPTION

The experiments that were performed were completed by placing a 1.0  $\mu\text{L}$  droplet of solution on a cleaned slide and using PIV analysis to observe the velocity magnitude and vorticity of the sample. A video of a length of one minute was taken to ensure consistency throughout all tests. The experimental process is consistent throughout all tests, however, the solutions used varied. There were six different tests completed and within each one, a variety of solutions were used. A detailed explanation of each test follows:

1. Distillation and Maturation: The purpose of this comparison was to differentiate the effects of congeners from the distillation and maturation process that goes into American Whiskey, to a control ethanol-water solution. Here a (a) binary mixture of ethanol and deionized (DI) water was compared to (b) unaged whiskey (Buffalo Trace White Dog) and (c) a Kentucky bourbon, Buffalo Trace (BT). All samples were diluted to 25% ABV.

2. Proof: The purpose of this comparison was to determine the effects of diluting American Whiskey from a higher proof solution with DI water. Here Buffalo Trace was tested at (a)



35% (b) 25% and (c) 15% ABV. The motivation of this test stems from the qualitative understanding that at (a) 35% ABV whiskey webs do not form and tend to form thin films, at (b) 25% ABV whiskey webs form and (c) at 15% ABV whiskey webs do not form and tend to form the well-known coffee-ring affect (Williams 2018, Brown & Carrithers 2019 submitted).

3. Surfactants: The purpose of this comparison was to analyze the effects of additional surfactant concentration in an American Whiskey. Here Buffalo Trace was used throughout all the experiments at 25% ABV where (a) no surfactants were added, (b) 0.005%wt of surfactant was added and in (c) 0.010%wt surfactant was added. This test is motivated by the results that added surfactant at concentration of 0.005%wt disrupted the web formation process for a normal web- producing American whiskey (Brown & Carrithers 2019 submitted). This test is to reveal what effect the surfactant has on the chaotic portion of the evaporation.

4. Filtration: The purpose of this comparison was to analyze the effects that filtration has on an American Whiskey. Two methods of filtration were tested along with a control. The American Whiskey tested was Staggy Jr. The control was the Staggy Jr. (a) unfiltered sample followed by (b) a non-chilled filtered sample, and (c) a chill filtered sample. This work was inspired by a complementary structured research project conducted at the University of Louisville by Katrina Boon (Boone 2019)e. (Fall 2018, ME 645, Factors that Influence Whiskey Webs)

5. Congeners: The purpose of this comparison was to isolate the effect that congeners have to the evaporation while not reducing the volatile components with a reduction in ABV. Since congeners were of interest, Booker's was chosen as an unfiltered product. The two

samples tested were (a) a control of Booker's and (b) a 50/50 volumetric mixture of the binary solution described in test 1 and Booker's. All samples were diluted to 25% ABV.

6. Whiskey Webs: The purpose of this comparison was to see if there is a significantly different 2D fluid velocity field produced by two qualitatively different whiskey web pattern (Williams 2018, Brown & Carrithers 2019 submitted). The two samples prepared were (a) Jim Beam Single Barrel and (b) Makers Mark Cask Strength. Both samples were diluted to 25% ABV.

### C. SAMPLE PREPARATION

#### 1. All Experiments (1-6)

All samples contained red fluorescent 1.0 $\mu$ m polymer microspheres (Fluoro-max 1% solids ( $\%_{fp}$ ) fluorescent particles for flow visualization. To keep the seed concentration consistent throughout all tests an arbitrary, but constant, value of fluorescent particles ( $Vol_{fp}$ ) were used, 5  $\mu$ L. Using the following equation

$$\frac{(\%_{fp} * Vol_{fp})}{(Vol_{sol} + Vol_{fp})} = \% Solids \quad (1)$$

where  $Vol_{sol}$  is the volume of the solution added to the particles and  $\% Solids$  is a constant that is recorded in Table III. This concentration value was first steered by values found in literature that also performed PIV analysis of a sessile droplet. A test solution was then diluted until the results lead to acceptable values. A lab member who regularly performs PIV consulted and agreed that the value chosen was acceptable. However, the optimal particle concentration was not of interest so it cannot be assumed. This concentration

however was held constant so any effect the particles had on the evaporation was constant between all tests.  $Vol_{Sol}$  can be solved for and substituted into

$$Vol_{Total} = Vol_{fp} + Vol_{Sol} \quad (2)$$

to find the total volume,  $Vol_{Total}$ . This value was held constant throughout all six tests.

After finding  $Vol_{Sol}$  the equation

$$Vol_{Sol} = Vol_{DI} + Vol_{ABV} \quad (3)$$

describes the relationship between  $Vol_{DI}$ , the volume of DI water used and  $Vol_{ABV}$ , the volume of any solutions that contain alcohol. The proof of an American bourbon or alcohol is

$$proof = 2 * ABV. \quad (4)$$

All the American whiskeys and alcohols used in the experiments have initial proofs above the values of interest in this study such that

$$Vol_{0\ proof} = V_{ABV} * \frac{(proof_{initial} - proof_{final})}{(proof_{final})} \quad (5)$$

describes the necessary amount of fluid that has zero proof,  $Vol_{0\ proof}$ , to dilute the initial alcohol volume,  $V_{ABV}$ , from its initial proof to the desired final proof. Where  $proof_{initial}$  is the initial proof of the solution and  $proof_{final}$  is the desired final proof that is being tested. Substituting (3) into (2) it can be stated as

$$Vol_{Total} = Vol_{fp} + Vol_{DI} + Vol_{ABV} \quad (6)$$

where

$$Vol_{0\ proof} = Vol_{fp} + Vol_{DI}. \quad (7)$$

Since  $Vol_{fp}$  has zero proof and will eventually be added to the total volume it has to be considered. To continue, (7) is substituted into (6) forming

$$Vol_{Total} = Vol_{0\ proof} + Vol_{ABV} \quad (8)$$

and finally substituting (5) into (8) and rearranging produces

$$Vol_{ABV} = \frac{Vol_{Total}}{1 + \frac{(proof_{initial} - proof_{final})}{(proof_{final})}} \quad (9)$$

After which substituting  $Vol_{ABV}$  into (8) finding  $Vol_{0\ proof}$  and finally substituting that into (7) finding  $Vol_{DI}$ . An example of such calculations are shown in Table II.

Table II

EXAMPLE OF WHISKEY WEB PIV SEED CONCENTRATION DILUTION TABLE

Variable Inputs		Variable Outputs (μL)	
$proof_{initial}$	100	$Vol_{Sol}$	495
$proof_{final}$	50.0	$Vol_{Total}$	500
% Solids	0.01	$Vol_{distalite}$	250
% <sub>sol</sub>	1.00	$Vol_{DI}$	245
$Vol_{fp}$ (μL)	5.00		

## 2. SURFACTANT EXPERIMENT (3)

In addition to controlling the proof and solids concentration, the Surfactant Experiment noted above requires a surfactant, Sodium Deoclyte Sulfate (SDS), to be added into the solution. The %wt of the SDS in relation to the weight of the entire solution is also a constraint.

The additional step began by determining the amount of solution that was needed to be added such that the weight concentration adheres to the additional constraint of

$$C_f = \frac{W_{SDS}}{W_{SDS} + W_{total}} \quad (10)$$

where  $C_f$  is the final %wt concentration and  $W_{SDS}$  is the weight of the SDS solution added and  $W_{total}$  is the total weight of the sample being tested. The  $W_{SDS}$  can be described as

$$W_{SDS} = \rho_{SDS} * V_{SDS} \quad (11)$$

where the  $\rho_{SDS}$  is the density of the SDS stock solution and  $V_{SDS}$  is the volume ( $\mu\text{L}$ ) of the SDS solution added to the sample. The  $W_{total}$  can be found after deriving the following equations

$$W_{total} = W_{ABV} + W_{H_2O} \quad (12)$$

where the  $W_{H_2O}$  is the weight of the water used to dilute the distillate and is found from

$$W_{H_2O} = V_{0proo} * \rho_{H_2O}. \quad (13)$$

The  $W_{ABV}$  is the weight of the solution containing alcohol and can be approximated from the weight of ethanol and water in the same ratio as its ABV by

$$W_{ABV} = \left( V_{ABV} * \rho_{eth} * \frac{ABV_i}{100} \right) + \left( V_{ABV} * \rho_{H_2O} * \left( \frac{100 - ABV_i}{100} \right) \right). \quad (14)$$

Substituting (5) into (13) and then that and (14)(12) into (12) results in

$$W_{total} = \left( V_{bourb} * \left( \frac{ABV_i - ABV_f}{ABV_f} \right) * \rho_{H_2O} \right) + \left( V_{Bourb} * \rho_{et} * \frac{ABV}{100} \right) + \left( V_{Bourb} * \rho_{H_2O} * \left( \frac{100 - ABV}{100} \right) \right). \quad (15)$$

After solving for  $W_{\text{total}}$  input that into (10) and solve for  $W_{\text{SDS}}$  where that is then input into (11) to finally solve for the volume of SDS,  $V_{\text{SDS}}$ , needed.

### 3. FILTRATION EXPERIMENT (4)

The samples were prepared the exact same way as was done in the structured research project (Fall 2018, ME 645, Factors that Influence Whiskey Webs). There were two samples that were filtered, each through a 0.45  $\mu\text{m}$  syringe filter. The one sample that was chilled was done at 0°C for 24 hours at bottle proof before being filtered (Fall 2018, ME 645, Factors that Influence Whiskey Webs). After the filtration process all the steps were taken to prepare the samples for analysis.

### D. EXPERIMENTAL SET-UP

After the solution were prepared, the hardware necessary for the experimentation was set up. A Nikon Eclipse Ti inverted microscope was used and a HiSpec 4G Mono high-speed camera was attached at its base, shown below in Figure 12b.

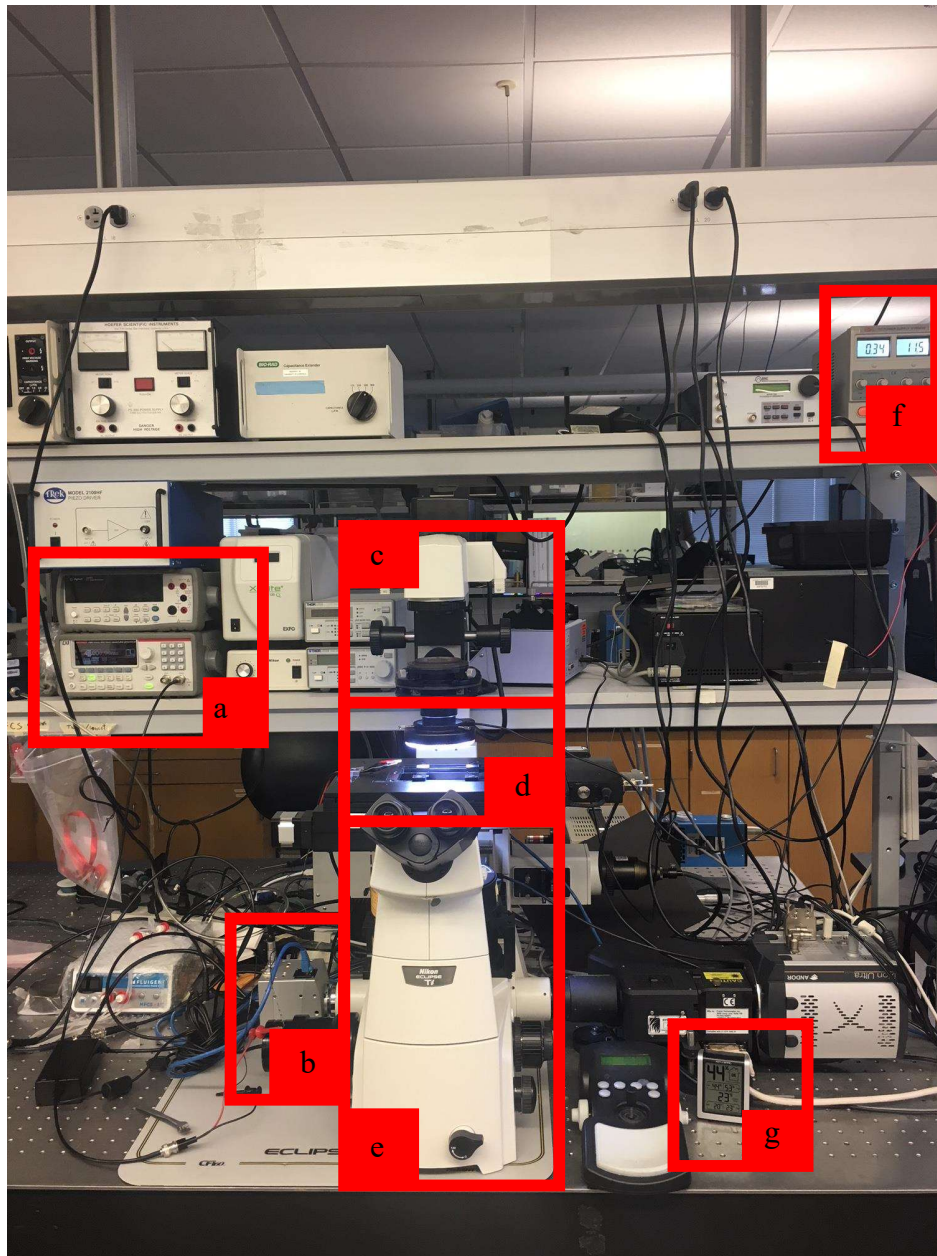


Figure 12- Overall Figure of the Mechanical Set-up a) Wave-form generator b) High-Speed camera c)LED ring light attaches and height can be adjusted d) platform where the slide sits above the lens e) base of the microscope where the 1.5X adjustment knob is located f)DC power supply for the LED ring light g) temperature and humidity sensor.

An LED ring light was attached above the stage providing the scattered light necessary to image the particles. It is powered by a DC power supply as shown in Figure 13.

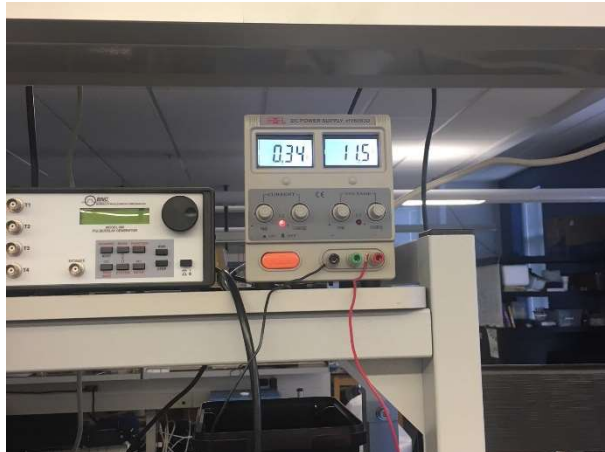


Figure 13 - DC power supply used for the ring light attachment.

The distance from the ring light to the stand was held constant for each test. The slides that are used are PTFE printed slides having 30 wells of 2 mm in diameter formed by a white mask made of Teflon shown in Figure 141414.



Figure 14 - White Teflon masked microscope slides.

The Teflon was used because of its hydrophobic qualities which provides a consistent boundary to constrain the droplet. One downside that became apparent after multiple tests is that the Teflon slides produced a halo effect at the outer portion of the droplet. This can be seen in Figure **Error! Reference source not found.**15.



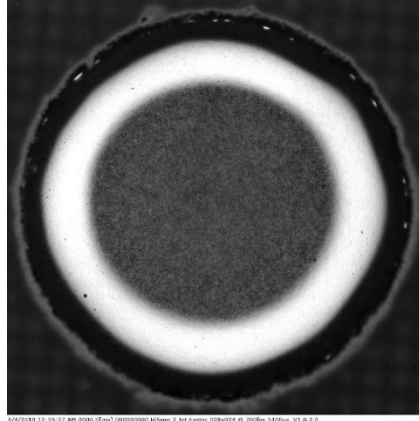


Figure 15 - Image taken by the mono colored high-speed camera. Notice the halo around the edge of the droplet. Steps were taken to attempt to minimize the thickness of halo but could not be eliminated.

Attempts were made to minimize this unwanted glare. Black Teflon masked slides were purchased with the same specs as the white Teflon slide described above. This was to attempt to eliminate the reflection of additional light, however, the manufacturing of the edges was jagged and not circular (Figure 16).

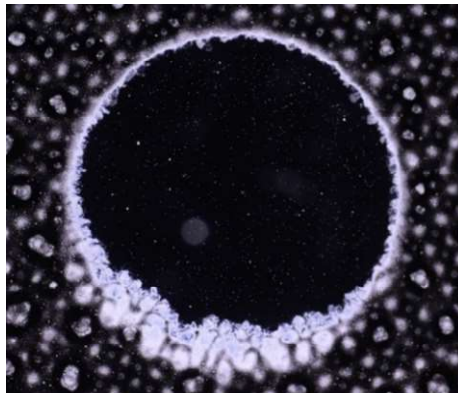


Figure 16 - Black printed PTFE mask which had poor quality, not used in study.

The poorly manufactured edges would have resulted in consistency issues as the shape of the droplet and contact angle are important parameters for sessile droplet evaporation. The mask still did not eliminate the haloing effect while only minimizing it. Another possible method that was explored as a solution to minimizing the halo around the droplet was to change the distance from the light source to the droplet. The further the light was to the droplet the less apparent the halo was, however, it also diminished the brightness of the particles, so a balance had to be determined such that the particles were still visible for the PIV to be successful.

A Nikon Plan Fluor lens with a 4X magnification and a 0.13 numerical aperture, NA, was used in series with the 1.5X setting on the microscope setup resulting in a total magnification of 6X.

The high-speed camera was connected to a computer via CAT5 and the camera was synchronized with the HiSpec control software. Within HiSpec there are various settings to control the camera's functions. The first parameter that is set is the region of interest (ROI). The ROI was set such that the entire droplet was visible during the duration of the test. The image size as defined by the ROI sets the maximum number of frames (*max frames*) that are able to be captured in a single video.

Table III

HIGH SPEED CAMERA SETTINGS

<i>fps</i>		700
<b>Shutter speed (<math>\mu s</math>)</b>		1400
<b>ROI (pixels)</b>	<b>X</b>	928
	<b>Y</b>	924

One of the parameters for the experiment was to have each video last for at least one minute. However, due to the high frames per second (*fps*) the memory would max out well before the one-minute requirement. To correct for this an external signal was utilized to program the camera to only take a fraction of the pictures. There was a setting on the software that would take,  $n_{frames}$ , at the set *fps*, every time it was triggered, either on a signal rise or fall. It was configured such that it would begin taking the images on the rise, or at the *peak* of the signal,  $\frac{n_{frames}}{peak}$ . Since the images are to be analyzed using PIV, the  $n_{frames}$  needs to be an even number because PIV analyzes in pairs. A Keithley 3390 50MHz Arbitrary waveform generator (Figure 16) was utilized to generate the signal that triggered the high-speed camera.

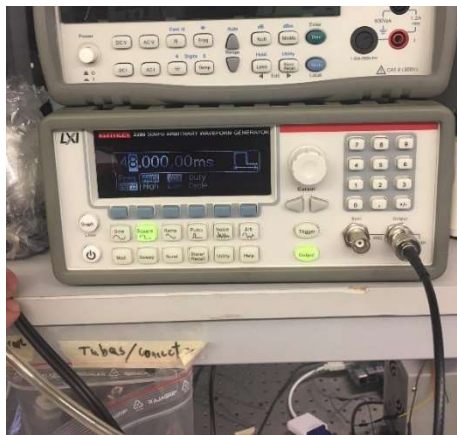


Figure 17 - Keithley 3390 50 MHz Arbitrary waveform generator used to trigger the high speed camera into taking the right amount of pictures.

The waveform generator was configured into the high-speed camera via pins 7 and 1 determined from Figure 18.


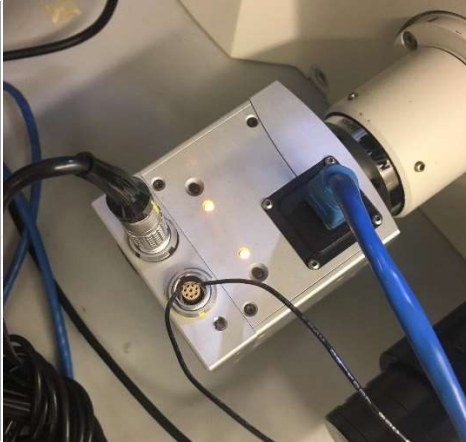
<b>Pinning of matching signal plug, (male, solder side)</b> 		select the plug according to your requirements, (right-angle plug/water-resistant etc.) under <a href="http://www.lemosa.com/">http://www.lemosa.com/</a> e.g. straight plug FGG.1B.308.CLAD52ZJ (Mounted socket in camera: EEG.1B.308.CLL)																											
<table border="1"> <thead> <tr> <th>Pin Nr.</th> <th>Signal Level</th> <th>Description</th> </tr> </thead> <tbody> <tr> <td>1</td> <td>GND</td> <td>GND</td> </tr> <tr> <td>2</td> <td>0...2.5V@ 1MΩ</td> <td>Analog input voltage, 8-Bit resolution</td> </tr> <tr> <td>3</td> <td>LVTTTL</td> <td>Sync Output / ARM</td> </tr> <tr> <td>4</td> <td>LVTTTL</td> <td>Digital Input 1</td> </tr> <tr> <td>5</td> <td>LVTTTL</td> <td>Digital Input 2</td> </tr> <tr> <td>6</td> <td>LVTTTL</td> <td>Digital Input 3/ IRIG-B Input (optional Cube4/5, 2 and HiSpec 2-HR)</td> </tr> <tr> <td>7</td> <td>LVTTTL</td> <td>Digital Input 4/ Trigger Input</td> </tr> <tr> <td>8</td> <td>LVTTTL</td> <td>SYNC Input</td> </tr> </tbody> </table>	Pin Nr.	Signal Level		Description	1	GND	GND	2	0...2.5V@ 1MΩ	Analog input voltage, 8-Bit resolution	3	LVTTTL	Sync Output / ARM	4	LVTTTL	Digital Input 1	5	LVTTTL	Digital Input 2	6	LVTTTL	Digital Input 3/ IRIG-B Input (optional Cube4/5, 2 and HiSpec 2-HR)	7	LVTTTL	Digital Input 4/ Trigger Input	8	LVTTTL	SYNC Input	
Pin Nr.	Signal Level	Description																											
1	GND	GND																											
2	0...2.5V@ 1MΩ	Analog input voltage, 8-Bit resolution																											
3	LVTTTL	Sync Output / ARM																											
4	LVTTTL	Digital Input 1																											
5	LVTTTL	Digital Input 2																											
6	LVTTTL	Digital Input 3/ IRIG-B Input (optional Cube4/5, 2 and HiSpec 2-HR)																											
7	LVTTTL	Digital Input 4/ Trigger Input																											
8	LVTTTL	SYNC Input																											

Figure 18: HiSpec Manual (Page 85) and actual image of wires connecting the waveform generator to the high-speed camera.

The signal specifications necessary for the trigger to be activated are recorded in Table IV33.

Table IV  
EXTERNAL TRIGGER SPECIFICATIONS

<b>Duty Cycle</b>	50%
<b>Low</b>	$0 V_{DC}$
<b><math>V_{os}</math></b>	$1.25 V_{DC}$
<b>High</b>	$2.50 V_{pp}$
<b>Amp</b>	$2.50 V_{pp}$
<b>Period</b>	48 ms

A square wave was chosen for simplistic reasons. The duty cycle is not important because the camera is only looking for the rise of the signal while the duration of the pulse width is irrelevant. The only variable that was left to solve for was the period of the signal. The minimum period would allow the user to capture the maximum frames while keeping the length of the video constant. While there are  $\frac{n_{frames}}{peak}$  taken it can be determined that the number of peaks must be limited to such that

$$peaks * \frac{n_{frames}}{peak} \leq max\ frames \quad (16)$$

is satisfied where the number of peaks can be expressed by

$$peaks = \frac{t_{total}}{T} \quad (17)$$

where  $T$  is the period of the signal. Substituting equation (2) into (1) and rearranging such that

$$T \geq \frac{t_{total}}{max\ frames} * \frac{n_{frames}}{peak} \quad (18)$$

shows the period that allows for the most frames taken at one minute's time. The time necessary to take  $n_{frames}$  is described by

$$t_{cap} = \frac{n_{frames} - 1}{fps} \quad (19)$$

where  $t_{cap}$  represents the theoretical minimum period possible under any conditions. The period,  $T$ , must be greater than  $t_{cap}$ . A figure showing the relation between images captured per trigger is shown in Figure 19.

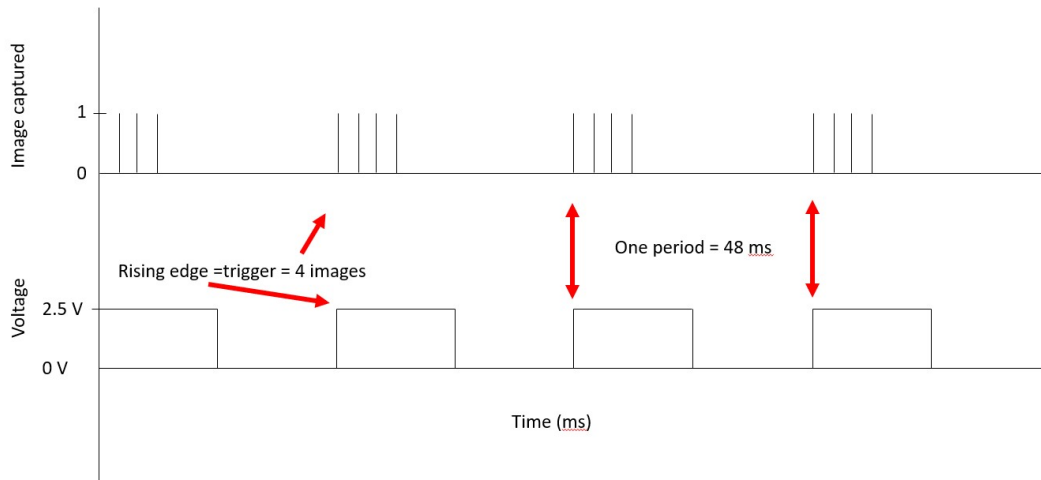


Figure 19 – Signal Diagram showing how the square wave is used to control the number of images captured.

The slides were cleaned by submerging each one into a petri dish filled with acetone and placing it in a Branson 1510 Ultrasonic Cleaner where it floated on the surface of the water for 5 minutes. Afterwards the slide was rinsed with acetone and then dried using compressed air.

Once all the pieces of the equipment were set up and the solutions were made, a 1.0  $\mu\text{L}$  droplet was extracted from the vial and deposited manually using a pipette rated for volumes between 1.0- 2.5  $\mu\text{L}$  onto the cleaned slide. An assistant in the lab operated the software and manually clicked the record button as soon as the droplet was deposited on the substrate. Any droplet that did not completely fill the well on the substrate was scraped and the test was repeated. An assistant was used to ensure the camera would start to record as soon as the droplet was placed on the substrate.

#### E. FRAME ANALYSIS

The analysis of the images were done in PIVlab within MATLAB 2019b (Thielicke 2014). To cut down on the computational time to analyze the frames only 10% of the images captured were used in the PIV analysis. A simple MATLAB (Supplementary Figure 1) code was constructed to only keep two out of every 20 frames. The program kept the first two images and then discarded the next 18 and proceeded as such throughout all the images captured. A single captured image is shown in Figure 155.

The images were then loaded into the program and the settings were determined in parallel with the fluorescent particle concentration. The interrogation areas were 32 & 16

pixels with a 50% step size for the first and second pass respectively. Calibration was done to determine the conversion between pixels to millimeters. A reference distance was drawn arbitrarily within the program where the program returns the length of the line in *pixels* seen in Figure 20.

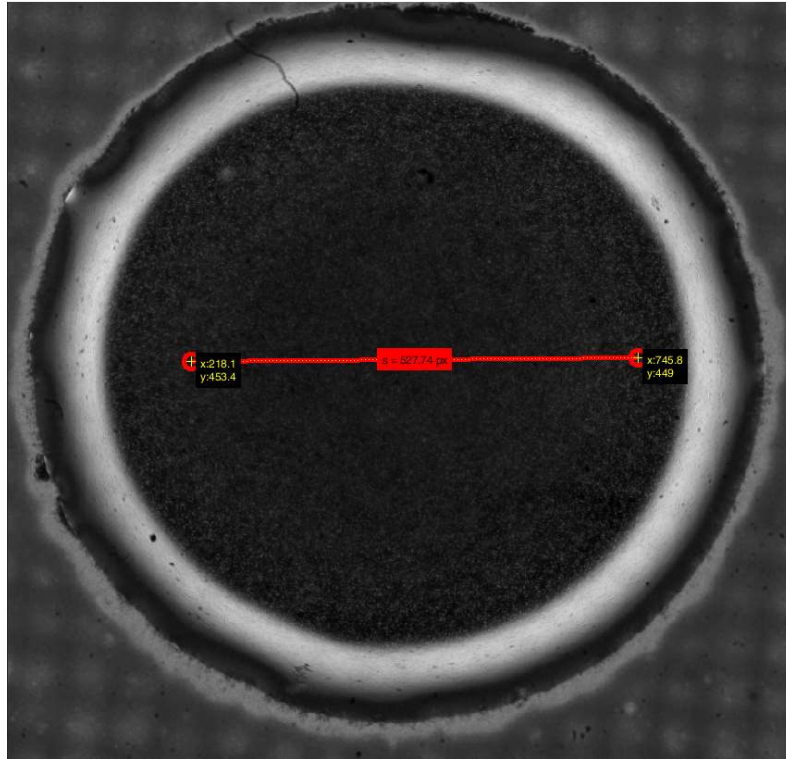


Figure 20 - An arbitrary line is drawn within the droplet. Any distance line can be used because of the formula below.

That pixel value is used in the following equation

$$real\ distance\ [mm] = pixels * \frac{14\mu m}{pixel} * \frac{1}{M} * \frac{1\ mm}{1000\ \mu m} \quad (20)$$

where the  $\frac{14\mu m}{pixel}$  is the actual pixel size of the camera and  $M$  is the magnification used in capturing the video which was known to be six. The images were then analyzed where the software compared images in pairs and produced a velocity field shown in Figure 21.

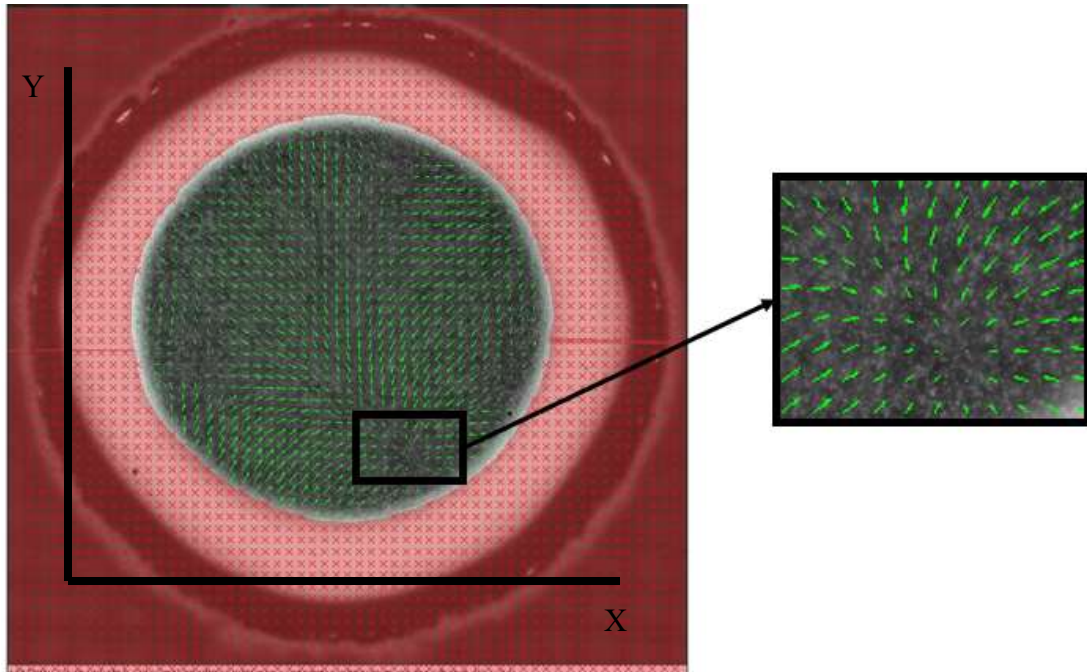


Figure 21 - Example of a masked and processed image pair is represented within PIVlab.

Postprocessing was performed via vector validation, manually imposing velocity limits. Limits were set at 1 cm/s for each component of velocity. The vectors that were outside of the velocity limits were removed from the data set. Velocity magnitudes (Fig. 22a) and vorticity (Fig. 22b) were derived in PIVlab, only one 2D velocity field was collected for each sample.



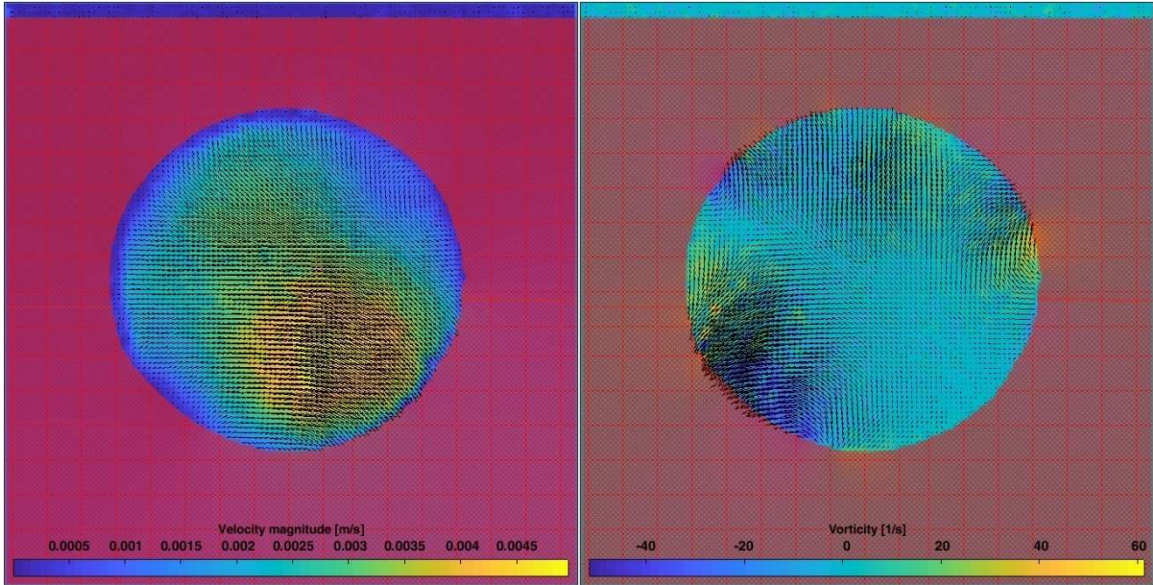


Figure 22: a) Velocity magnitude and b) vorticity images exported from PIVlabs

The image files of the velocity magnitude and vorticity results for each test were saved as an image file in addition to the data MAT file. The MAT file is able to be manipulated within MATLAB and contains the 2D velocity and vorticity fields for each image pair. Each 2D velocity and vorticity field are represented in MATLAB as a matrix sized 117 X 115. The size of the matrix was determined by the ‘step size’ of the interrogation window. Within each flow field, the data that is of interest within the chaotic flow is the vortices. Since only a small portion of the droplet exhibits the vortices, each frame’s vectors were ordered largest to smallest. Only the top percentage of the vectors were averaged to determine the single value representing that image pair in time. (Supplementary Code 2).

Analysis was performed to see if the percentage (20%,10% and 5%) of retained velocity vectors had any effect on the trend of the results (Figures 32, 33, 34). It was determined that the trends remained relatively constant the only difference being the scale of the fluid velocity (mm/s). This was intuitive being that the more data you include with

20%, it will inherently be the scaled down version of 5% because it includes 15% of the next smallest values. It was determined that 20% was sufficient and all further tests proceeded with only presenting such. This analysis was performed for each flow field contained within the array of cells that was contained within the MAT file. The length of each array was 1 X 252 and is correlated to the number of image pairs imported into the program. It was decided to represent the averaged fluid velocity over the entirety of the one-minute long test. This was done to highlight and compare the different samples both on their fluid velocity magnitude and fluid velocity over time. The time between each averaged velocity magnitude was 480 ms.

When analyzing both velocity magnitudes and vorticity for each experiment, the similarities between the trends are unmistakable. This can be explained as the equation of vorticity is

$$\omega = \frac{\partial v}{\partial x} - \frac{\partial u}{\partial y} \quad (21)$$

where  $v$  and  $u$  are the Y & X components of velocity respectively as seen in Figure 21 (J. Stamhuis and Videler 1995). Vorticity is directly related to velocity magnitude and seems to follow similar trends that the velocity magnitudes follow. This is shown in Figure 23 where velocity magnitudes (Figure 23a) had identical trends as vorticity (Fig. 23b). Therefore, to avoid presenting redundant data, results from the velocity magnitude data sets will only be presented in subsequent sections.

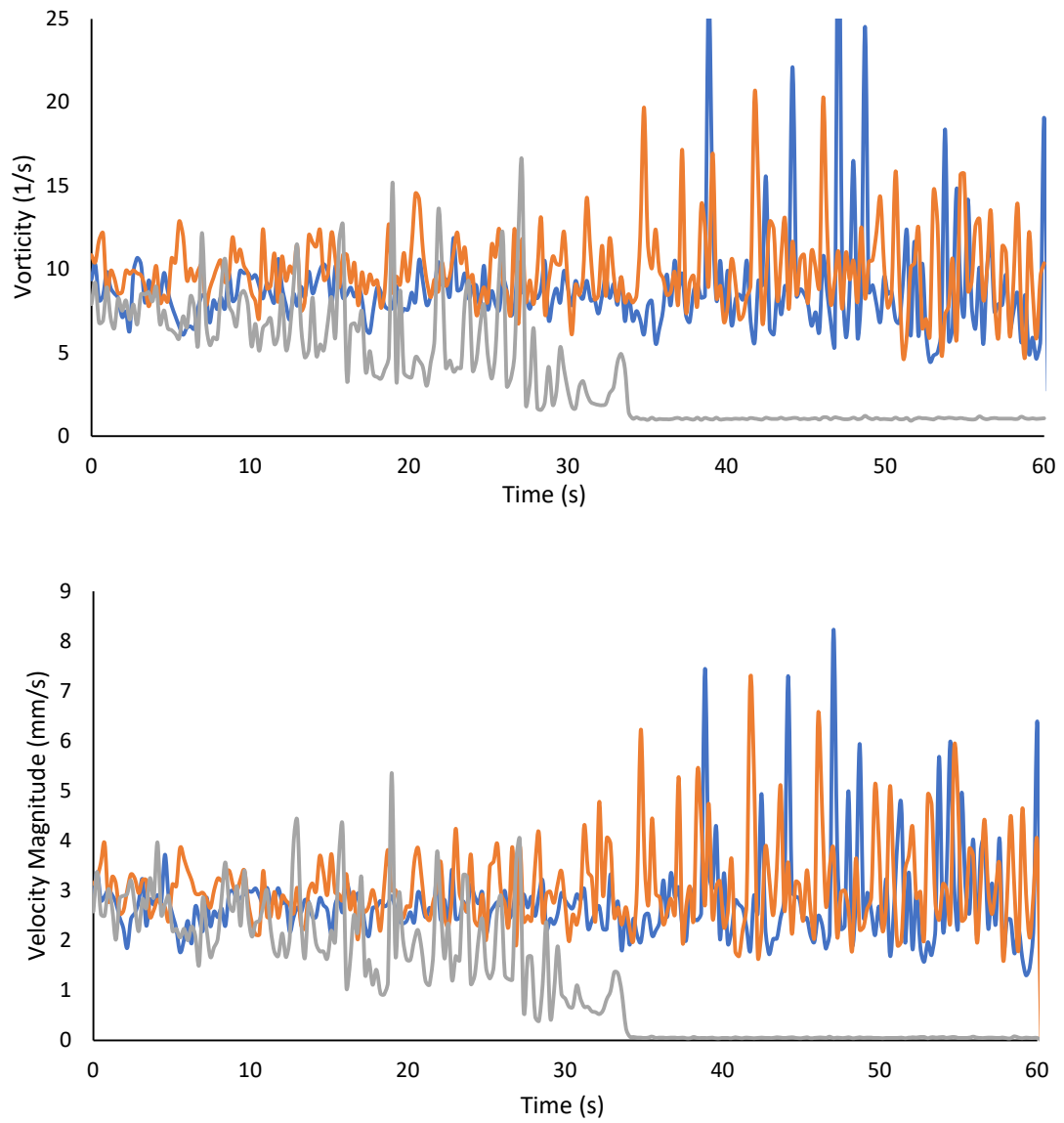


Figure 23. Vorticity (a) and Velocity Magnitude (b) data from the Distillation and Maturation experiment. Notice the trends between the two figures are almost identical to each other.

### III. RESULTS AND DISCUSISON

#### A. DISTILLATION AND MATURATION EXPERIMENT (1)

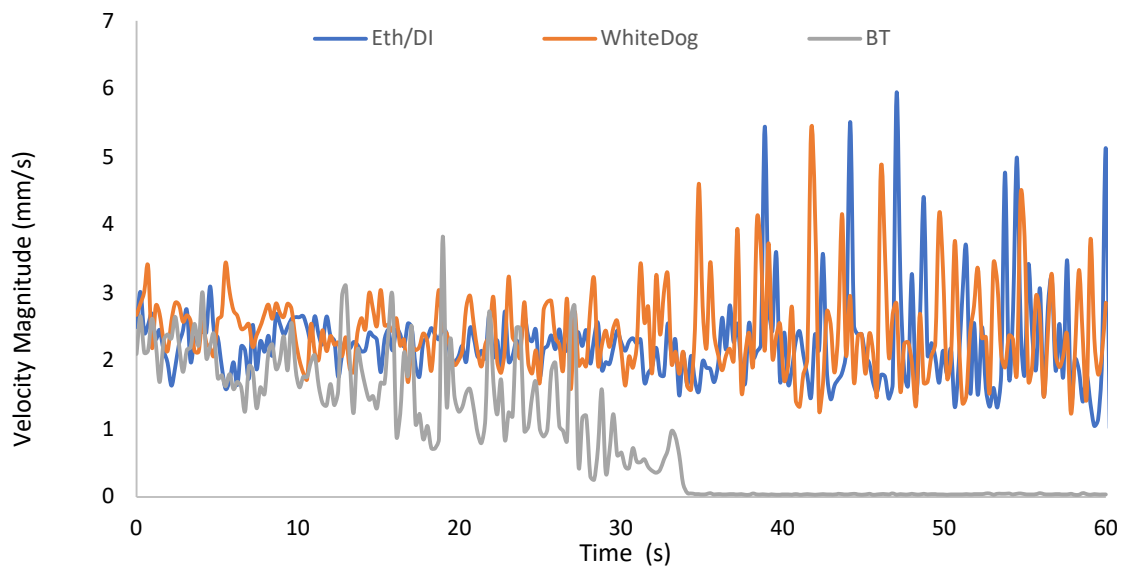


Figure 24: Distillation and maturation results.

The velocity magnitude and trends of such are very interesting for Experiment 1. The binary mixture and white dog were very similar in their magnitude and duration of chaotic

flow. The American whiskey, however, leveled out 35 seconds into the one-minute long video. This result shows that the aging of an American whiskey will suppress the chaotic flow duration of the evaporation. This result was especially interesting because there have been studies that claim that mature whiskeys can actually suppress the release of volatiles (ethanol evaporation) (Conner 1997, Piggott 1997, Boothroyd, Linforth et al. 2012). The magnitude of all three solutions tested started out around the same value and only after the American whiskey finished its chaotic flow were there significantly larger peaks for the white dog and ethanol. This result was similar to (Bennacer and Sefiane 2014) where they measured a spike in radial velocity at the end of the ethanol evaporation period. They speculated that this was due to the increased ethanol concentration gradients from some areas of the surface have significantly less ethanol.

### B. PROOF EXPERIMENT (2)

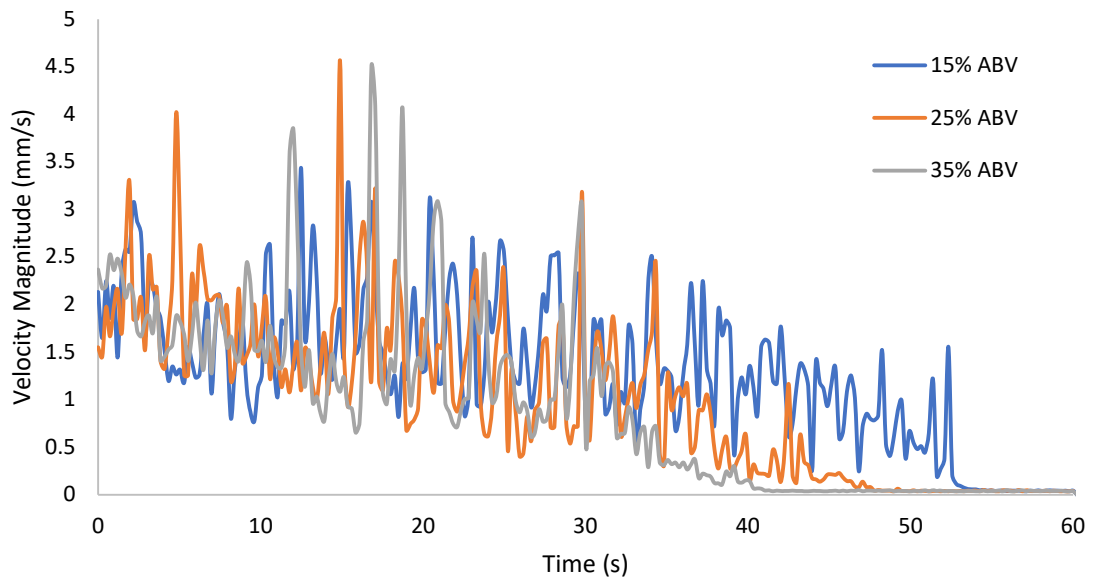


Figure 25 - Top 20% vectors for varied dilution of an American whiskey

The results from Figure 25 show that as dilution increases so does the duration of the chaotic flow due to the ethanol evaporation. This is intriguing because the more concentrated sample exhibited a shorter chaotic flow while velocity magnitude was relatively the same. Further, as the sample is diluted, the congeners themselves are also diluted which otherwise suppress sample volatility. This supports (K, L et al. 2003), where they observed a higher evaporation rate in a higher ABV sample than that lower concentration samples.

### C. SURFACTANT EXPERIMENT (3)

The presence of a surfactant in a solution has been used to suppress the coffee ring effect and to help understand the presence of a thin film for whiskey (Kim, Boulogne et al. 2016). Surfactants in a small concentration are known to overpower the Marangoni effects contributed by thermal induced flows (Hu and Larson 2005). It also has been shown to disrupt web formation and has been offered as the reason that the American whiskey Final Reserve aged 42 years does not produce a web pattern (Brown & Carrithers 2019 submitted). Results are below in Figure 26.

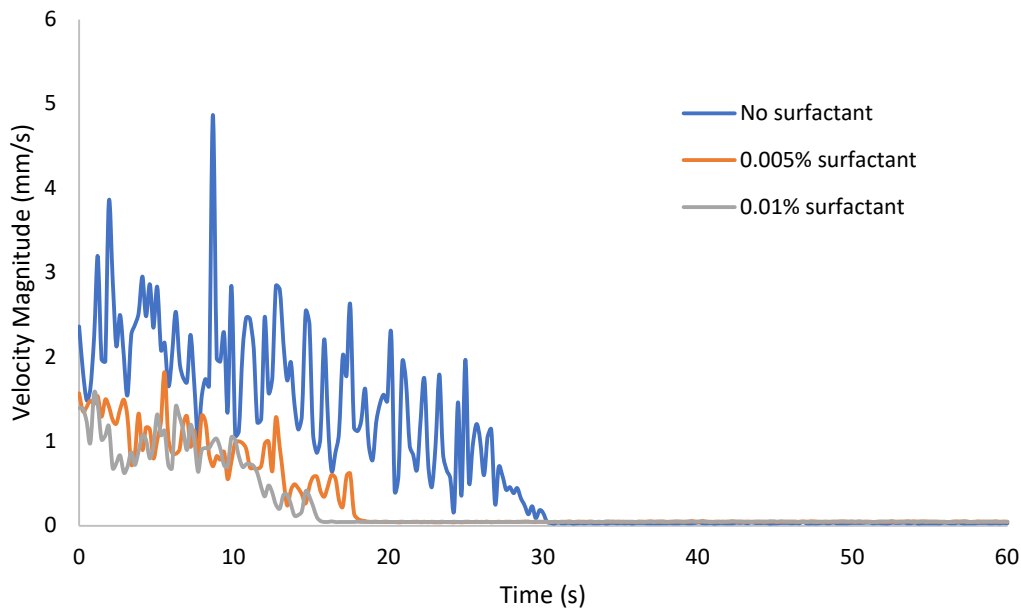


Figure 26: The magnitude of velocity of samples prepared with varied levels of SDS.

The SDS suppressed the magnitude and duration of the chaotic evaporative flow. The model conceived through reading Stone's paper was that the surfactant was increasing the chaotic nature and that adding additional surfactants only exacerbated the chaotic flow. Stone described a hierarchy of contributing parties to Marangoni flow, (a) solutal (b) surfactant and (c) thermal. By adding additional surfactant, it strengthened the effects of its Marangoni flow and resulted in the evaporating droplet entering into the surfactant dominated flow regime sooner. Additional surfactant can therefore be confidently linked to a reduction in fluid velocity and potentially a reduction in web formation.

#### D. FILTRATION EXPERIMENT (4)

The American whiskey industry has various ways to differentiate their product from other competitors. One such method is their filtration process. The results of the structured research project showed that filtration effected the density of web-like structures produced after complete evaporation (Fall 2018, ME 645, Factors that Influence Whiskey Webs). To gain insight into comparing the fluid velocity of the various samples from the structured research project, the experiment was repeated the results are in Figure 2727.

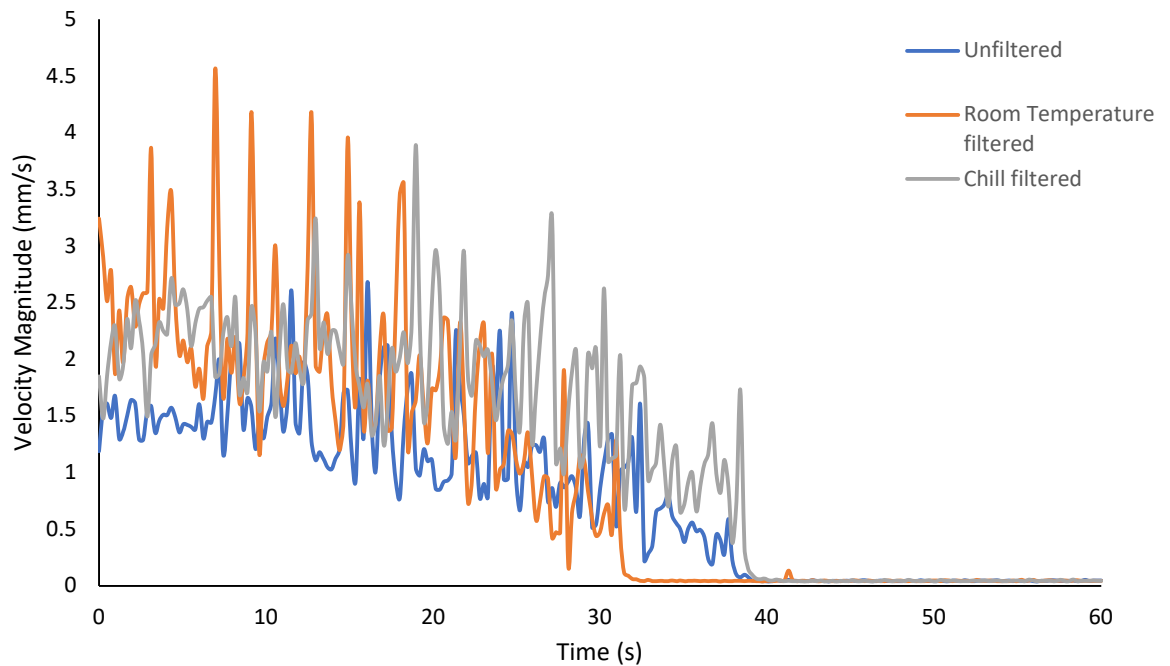


Figure 27 - Velocity Magnitude of solutions after various method of filtration as well as a control.

An additional sample of an American whiskey filtered at room temperature was added to see if there were any noticeable differences between the chill filtered solution. Both



filtered samples exhibited higher magnitudes of velocity, however, it is interesting that the chill filtration sample chaotic flow ended about the same time as the unfiltered sample. Whereas the room temperature filtered sample ended its chaotic flow about 10 seconds before the other two samples. The higher magnitude of velocity in the filtered samples align with the result from the previous work, producing more web-like structure than that of its unfiltered counterpart. It was believed that the increased fluid velocity was linked to increased web-like structures and these results help to support that claim. While this study's purpose was not to look too heavily into the difference between chill filtration and normal filtration, it brings up an interesting result that could be explored further along with more statistical repeatability tests.

#### E. CONGENERS EXPERIMENT (5)

The dilution of congeners is another attempt to explore the effect of constituents derived from the distillation and maturation process. The experiment was designed to keep the amount of ethanol consistent throughout all tests (25% ABV) while only changing the concentration of congeners. The results are shown in Figure 28.

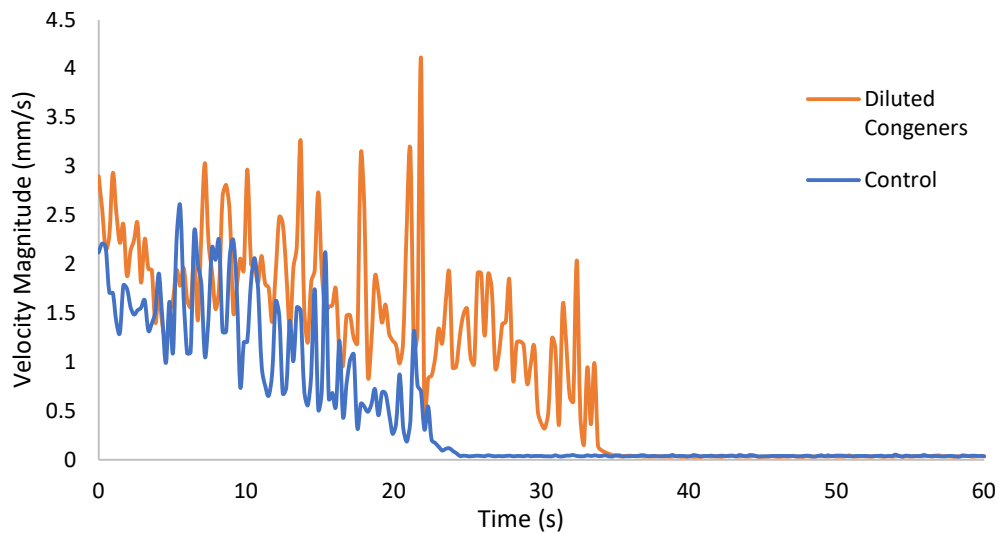


Figure 28 - Velocity Magnitude of an unfiltered American whiskey and one that is held at the same ABV while diluting the congeners present in the solution.

The experiment again showed that as the present congeners were diluted, the less suppressed the chaotic flow became. However, the increase of the velocity magnitude does not inherently mean that there will be an increase in web formations as described earlier. The conditions that need to be met for web-like structures to form from the evaporation of American whiskey are detailed and specific (Brown & Carrithers 2019 submitted). All components need to be considered and while this process increased fluid velocity, it also had drastically decreased the wood derived components necessary for a monolayer to form, collapse and subsequently forming the web-like structures.

#### F. WHISKEY WEBS EXPERIEMENT (6)

The last experiment tested was that of two different American whiskeys that exhibited two distinctly different web patterns. The first American whiskey was that of Maker's

Mark Cask Strength whose web pattern resulted from shorter “webby” web-like structures shown in Figure 8a. The other American whiskey that was tested was a Jim Beam Single Barrel whose web pattern comprised of long thick strands, Figure 8c. It was theorized that whiskey webs are formed during one of two droplet evaporation phases: during the chaotic ethanol evaporation and/or that of the bulk fluid evaporation (Brown & Carrithers 2019 submitted). The process that drives the web-like structure formation in the chaotic flow evaporation is from the fluid velocity and vortices generating the surface pressure necessary for monolayer collapse. The driving force behind web formation in the bulk fluid evaporation is the decreased surface area resulting from the surface area to cross sectional area that the droplet had contact with the substrate. The slow build of pressure from this process ultimately reached the collapse pressure of the monolayer and collapse ensues. This process sounds very similar to the slow collapse mechanisms described by others who study monolayer collapse (Ybert, Lu et al. 2002). The proposed collapse procedure for the chaotic flow region resemble the high compression rate and high surface or low surface pressure described by the “multiple folds” and “giant folds”. Since this study does not have a way to measure the pressure explicitly it will not be able to distinguish between the pressures and compression rate related to collapse mechanisms; however, these results could help better understand what is going on in different American whiskey products and lead to further testing. The results are shown in Figure 29.

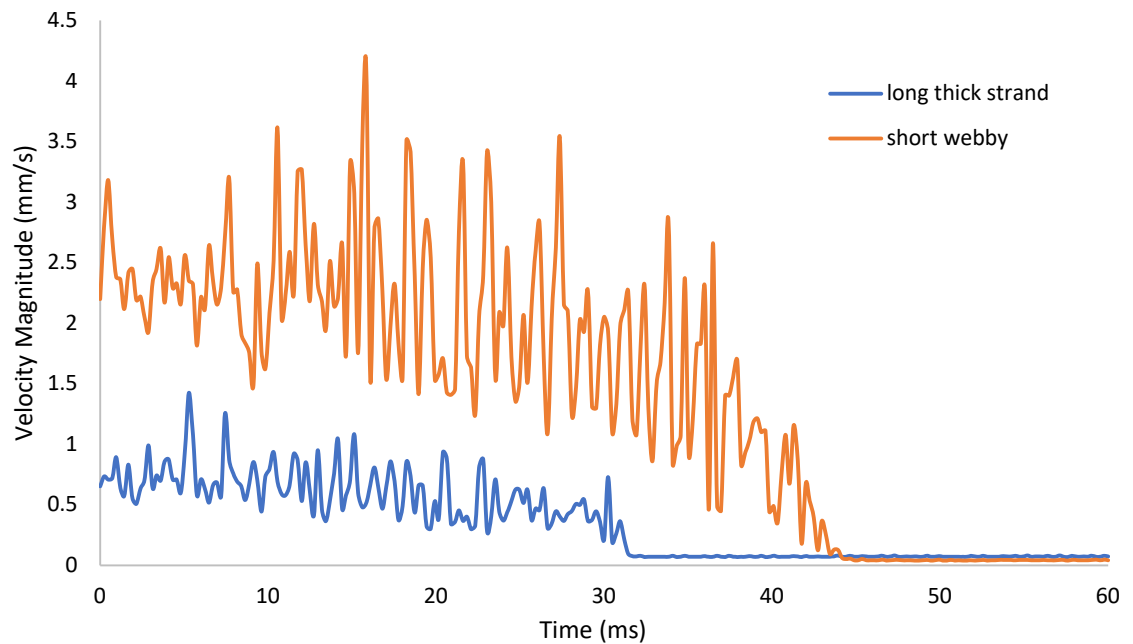


Figure 29 - Velocity Magnitude of two distinctly different web-like structures that make up two distinctly different whiskey web patterns.

The Jim Beam sample had a noticeably smaller magnitude of velocity and duration of chaotic flow. This result is interesting because it aligns well to the notion that Jim Beam Single Barrel does not produce web-like structures during the chaotic flow period of evaporation but produces its webs from the bulk fluid evaporation. The Maker's Mark Cask Strength sample on the other hand had significantly higher magnitude of velocity and for a longer period of time. This also supports the assertion that Makers Mark produces the majority of its webs during the chaotic evaporation period. Although there is a correlation, other differentiating factors between samples such as filtration, mash bill and aging could have also influenced the results. However, these results lead one to believe that the uniqueness of the web pattern is linked to the fluid flow during the ethanol evaporation of an American whiskey.

## 1. REPEATABILITY EXPERIEMENT

There are many sources of error and places for improvement in further studies. One example is conducting these trials under controlled and repeatable temperature and humidity. Each experimental trial was conducted in the same session on the same slide, though each experimental was conducted on different days. However, the following test was performed to demonstrate the repeatability of evaporation behavior of a sample for consistent same environmental conditions. In this test, Buffalo Trace was prepared in the exact same steps as described in Sample Preparation to 25% ABV. Three droplets were analyzed from the same stock solution to determine the repeatability. These results show that the velocity magnitude and duration of all three samples are consistent (Figure 30).

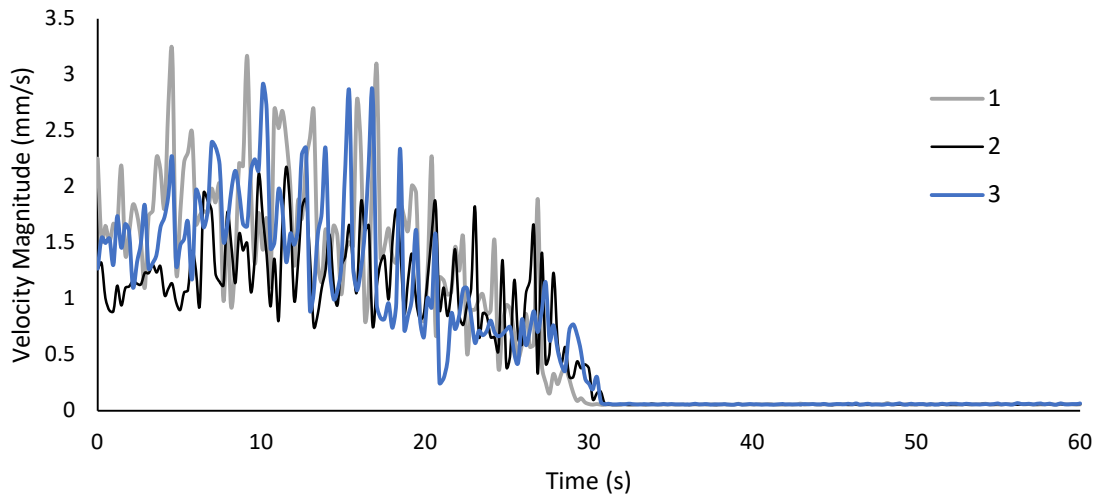


Figure 30 - Repeatability test 25% ABV Buffalo Trace. All three sample are consistent within the magnitude and duration of chaotic flow.

This paper lays out a process to analyze a 2D fluid velocity field of a volatile evaporated sessile droplet of a diluted American whiskey. The process outlined provides an underestimate of the velocity magnitude and vorticity while still being able to compare

the effects of variables between tests. This is an underestimate because the field being measured is a 2D field however the evaporation is in 3D, any fluid velocity in the z direction is lost as shown in Figure 31. It was shown that results can be used to compare between tests however, the environmental conditions, human error in placing the droplets on the slides, hydrophobicity differences as well as slight differences in solution concentration effect consistency between tests.

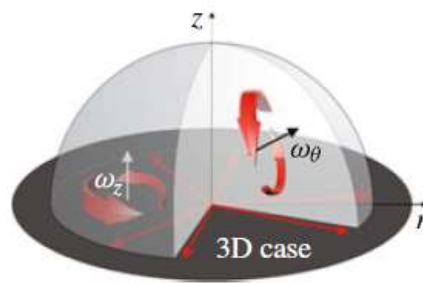


Figure 31 - Schematic showing the vortices are 3D not just 2D. Figure reproduced from (Bennacer and Sefiane 2014).

#### IV. CONCLUSION

Accomplished within this work was a process to gather data to better understand the internal fluid motion of an evaporating American whiskey droplet. It further allows a fluid flow comparison between samples that are altered to isolate a single parameter of interest. This provides a roadmap for more in depth analysis where someone would analyze a single parameters effect on the fluid velocity. Additionally, this study is building the base of understanding to explore how fluid motion of an evaporating American whiskey droplet can be linked to a whiskey web pattern. This could ultimately be used to link web-like structure types to monolayer collapse mechanisms. Which in turn could then be used to categorize whiskey characteristics to qualitative surface patterns.

This work is multidisciplinary in nature and ties multiple different topics (binary solution evaporation, colloidal self-assembly, monolayer collapse, etc) together that have never been studied in conjunction with one another. It also has the potential to engage and educate the community in colloidal science, microfluids and in the bigger

picture science and engineering. The whiskey web patterns are aesthetically pleasing and have been accepted as art pieces around the country. The community outreach has been a great point of expanding the skill of conveying complex ideas to multiple different education levels.

The results from the study confirm that internal fluid flow is affected by changes to parameters (maturation, distillation, proof, etc ....) and provides data to support this. The first test shows that not until a product is matured in a new oak barrel, not just distilled does the suppression of the chaotic flow occur. This further support the assertion that the maturation process is a fixture for whiskey webs to form. This result does not look at how aging across multiple different years changes the suppression of the chaotic flow.

The dilution of an American whiskey reduces the ABV while also reducing the congeners concentration. The results show that the higher proof American whiskey have suppressed chaotic flow when comparing it to their diluted counterparts, where the congener test show that the congeners suppress the chaotic flow independent of ABV.

Additional surfactants within a solution increases the strength of the surfactant-based Marangoni flow. This reduced the velocity magnitude of the chaotic flow. This can help to understand potentially why qualitative observations where the same concentration of SDS was added to a normally whiskey web producing solution and no webs formed. This supports the assertion that web-like structures are formed during the ethanol evaporation period but only if the chaotic flow produced sufficient surface pressure from the fluid motion underneath for the monolayer that rests on the air-liquid interface to collapse. This would support the idea that a suppressed chaotic flow would produce less or no webs altogether.



The process of filtration has been shown to change the quantity of web patterns produced from the same sample. This work showed data of fluid velocity for unfiltered and filtered samples. The increase in fluid velocity of the filtered samples again support the claim that increased velocity magnitude translates to additional web-like structures being formed during the ethanol evaporation.

The most interesting result was the clear distinction in fluid velocity between the qualitatively different web-like structured whiskey web patterned samples. This is groundwork for additional analysis to better distinguish and correlate monolayer collapse mechanisms to whiskey web-like structures. A summarized list of results are shown in Table

Table V

## SUMMARIZED RESULTS

Experiment #	Variable Isolated	Takeaway
1	Maturation and Distillation	Maturation suppresses the chaotic flow duration.
2	Alcohol by Volume (ABV)	Dilution extends the duration of chaotic flow.
3	Surfactant (SDS)	Additional surfactant in a solution increases the strength of the surfactant Marangoni flow which more quickly overcomes the solutal Marangoni flow (ethanol). This ultimately suppresses the length of the chaotic flow duration and strength.
4	Filtration	Filtration leads to a greater magnitude of fluid velocity during the chaotic flow.
5	Congeners	Congeners suppress duration of chaotic flow independent of ethanol concentration.
6	Whiskey web pattern	Two distinct web-like structures have distinctively different fluid velocities
	Repeatability	Tests on the same slide, same sample, same environmental conditions produce very similar fluid velocity magnitudes and duration of chaotic flow

## V. RECOMMENDATIONS

Future work in the field could go a lot of different directions. This study was conducted so that as many variables as possible were held constant, however, a statistical analysis of these results would be beneficial to provide a confidence interval (percentage) for these results. Another hurdle that had to be overcome is that due to the geometry of the droplet there was a white halo around the edge of the droplet that shielded a percentage of the droplet and subsequently data. With the most chaotic flow around the edge, undoubtedly a large portion of the most chaotic flow was lost. A possible solution around this is to purchase a chromatic high-speed camera and use the fluorescent particles to their full potential. This can be visualized from a video taken for qualitative purposes early on in the research (Brown & Carrithers 2019 Submitted). In the video there is no halo around the edge because a filter is used that only captures the red fluorescence and screens out all other light.

Work that would be motivated from the results presented here would encompass looking into quantifying the pressure for each type of webs. If it can be confirmed that collapse mechanisms can be confidently correlated to web-like structures, then it could be possible to begin to group American whiskey's into categories based upon their web-like structures. It would need further testing, but it would be very interesting if patterns began to form, such as all rye whiskey or all single barrels producing the same type of web structures. This qualitative observation could then lend itself to becoming a characteristic of American whiskey.

Another avenue that would be interesting to explore further would be a more extensive analysis into the effect of filtration and the results between chill filtration and room temperature filtration.

Also, while the first test showed that maturation suppressed the chaotic flow when comparing the results to that of unaged "white dog". It did not show the relationship between the degree of suppression and the age. An additional test where multiple ages of the same product would yield potential insight in the degree of suppression as a product is aged and would highlight whether the trend is linear as would be expected from the two data points collected.

The last interesting piece that was discovered through literature review is that monolayers tend to fold in the same location when compressed and relaxed in a cyclical manner. This fascinating observation in a study done implies that the monolayer has a predisposition to folding in a certain location(Ybert, Lu et al. 2002). This is interesting when taking that into context with the qualitatively repeatable web patterns from the same sample. It would be fascinating to be able to compress and relax a sample of American

whiskey in a Langmuir trough and observe if the location of the fold are in similar locations between multiple tests of the same sample.

## VI. APPENDICES

Supplementary Code 1 - MATLAB code that cuts down the image pairs from the max frame number to  $\frac{1}{10}$ <sup>th</sup> of that number.

```
pathname =  
E:\Repeatability\6X_7152019_65349_PM';%original folder  
location  
ext = '*.tiff'; % extension you care about  
d = dir(fullfile(pathname,ext)); % get the relevant  
directory contents  
filenames = {d(:).name}  
'; % relevant filenames  
  
mask1 =  
~cellfun('isempty',regexp(filenames,'6X000000[0-5][0-  
9][02468][01]'));  
%filter that only accepts images that have images named  
0 and 1 in the one place and even in the tens place.  
  
src = fullfile(pathname,filenames(mask1));  
dest =  
fullfile('E:\Repeatability\10p_3',filenames(mask1));%  
destination folder location  
cellfun(@copyfile,src,dest);%copies over file
```

Supplementary Code 2 - MATLAB code that extracts the data from the MAT file and converts it into a single data point per frame.

```
s = length(velocity_magnitude); % allows for a dynamic
analysis of various number of frames
total_M_results = []; % vector initialization for top
XX number of results
total_V_results = [];
mean_mag_data = zeros(1, length(velocity_magnitude));
mean_vort_data = zeros(1, length(velocity_magnitude));
%total_M_results = zeros(length(velocity_magnitude),
50); % trying to preallocate space
%total_V_results = zeros(length(velocity_magnitude),
50);

    for i= 1:s

        Ms =
sort(velocity_magnitude{i,1}(:), 'descend'); %extracts
matrix from array of file exported from PIVlab and
orders them in descending order
        result = Ms(1:ceil(length(Ms)*0.10)); %copies
over the top XX% of the values
        mean_mag_data(i) = mean(result); %averages the
results and finds average value for each frame and adds
it to a new array

        Vs = sort(vorticity{i,1}(:), 'descend'); %
performs the same operation but for vorticity
        vort_result = Vs(1:ceil(length(Vs)*0.10));
        mean_vort_data(i) = mean(vort_result);

        % this is used to find the top 50 vectors/frame
and assembling them
        % into a matrix
        topM_50 = Ms(1:50); %top 50
        topM_50_row = topM_50'; % transpose column into
a row
        total_M_results = [total_M_results;
topM_50_row]; % builds matrix [#frames X 50]

        topV_50 = Vs(1:50);
```

```

        topV_50_row = topV_50';
        total_V_results = [total_V_results;
topV_50_row];

    end
    %-----
-----
    % this finds the max 10 vectors from all the frames
for each test.
    Max_Mag_list = sort(total_M_results(:), 'descend');
    overall_test_max_Mag = Max_Mag_list(1:10);

    Max_Vort_list = sort(total_V_results(:), 'descend');
    overall_test_max_Vort = Max_Vort_list(1:10);
    %-----
-----
    % transposes list for excel export
    mag_data = mean_mag_data';
    vort_data = mean_vort_data';

```



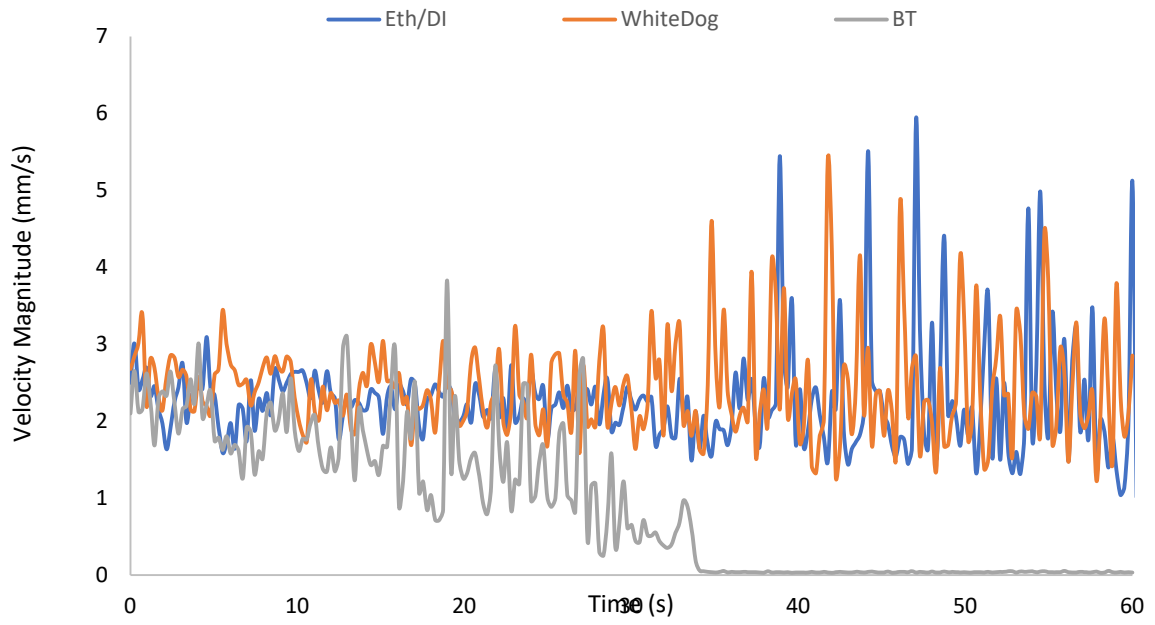


Figure 32: Experiment 1. Top 20% velocity magnitude versus time

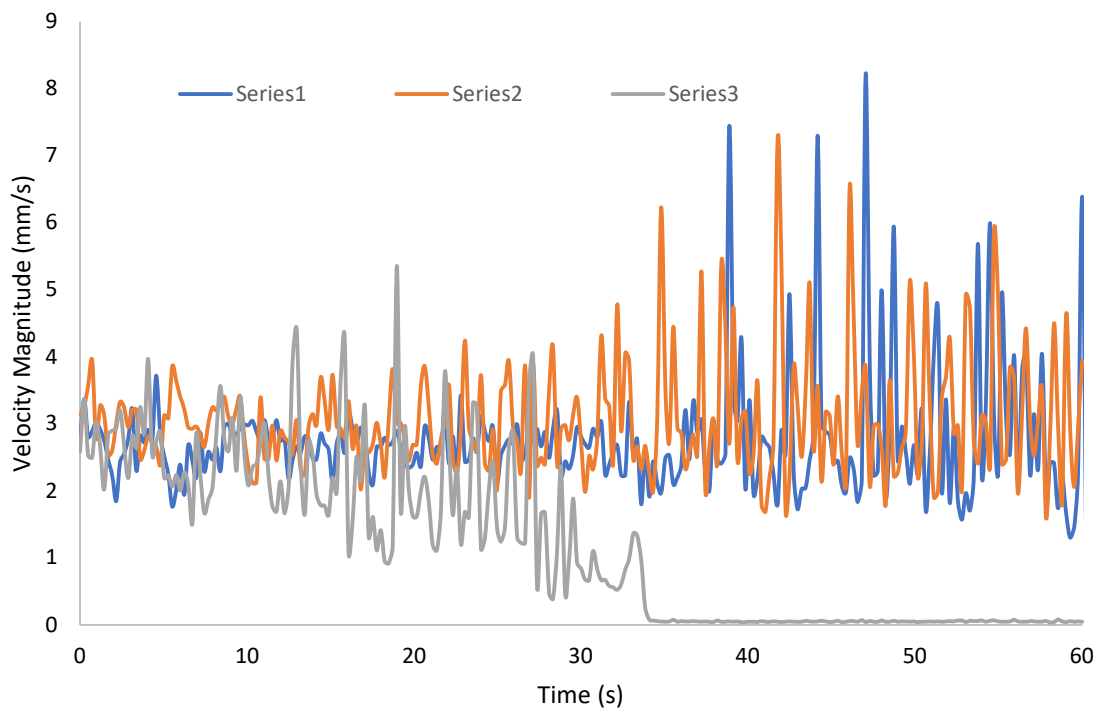


Figure 33: Experiment 1. Top 10% velocity magnitude versus time

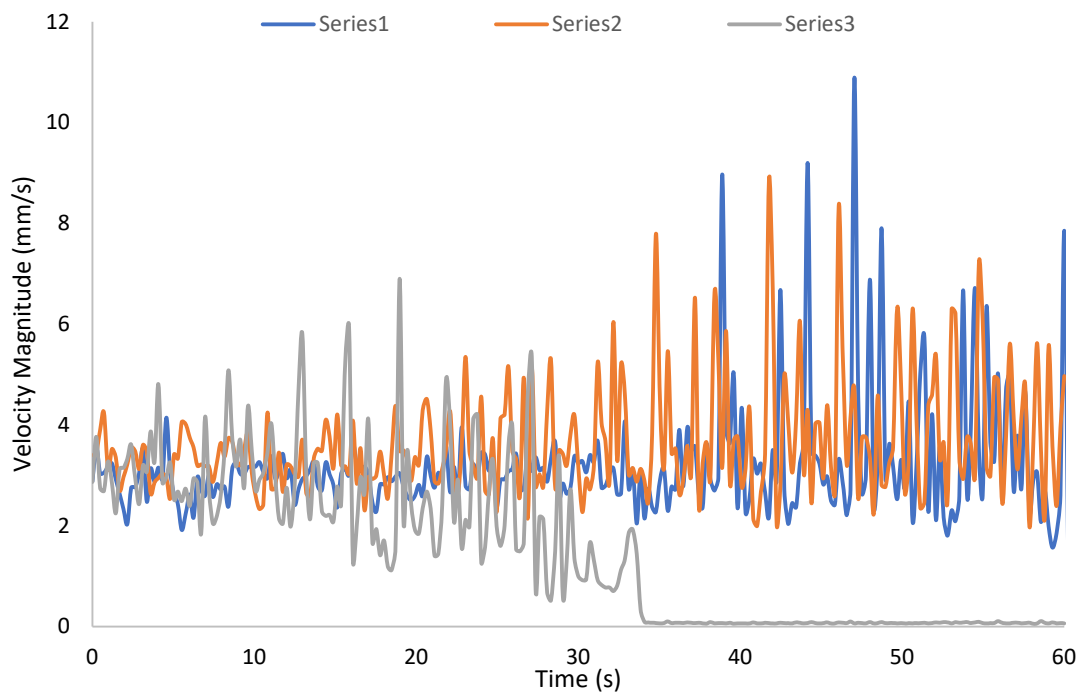


Figure 34: Experiment 1. Top 5% velocity magnitude versus time

## VII. LIST OF REFERENCES

- Bennacer, R. and K. Sefiane (2014). "Vortices, dissipation and flow transition in volatile binary drops." Journal of Fluid Mechanics **749**: 649-665.
- Blodgett, K. B. (1935). "Films Built by Depositing Successive Monomolecular Layers on a Solid Surface." Journal of the American Chemical Society **57**(6): 1007-1022.
- Blodgett, K. B. and I. Langmuir (1937). "Built-Up Films of Barium Stearate and Their Optical Properties." Physical Review **51**(11): 964-982.
- Boone, K. (2019). "Factors that Influence Whiskey Webs."
- Boothroyd, E. L., R. S. T. Linforth and D. J. Cook (2012). "Effects of Ethanol and Long-Chain Ethyl Ester Concentrations on Volatile Partitioning in a Whisky Model System." Journal of Agricultural and Food Chemistry **60**(40): 9959-9966.
- Brown, M. J., Carrithers, Adam D. Rashed, Mohamed Z., Islam, Sabina, Velev, Orlin, Williams, Stuart J. (2019). "Multiscale self-assembly of unique web-like structures from evaporated drops of dilute American whiskeys (Submitted)."
- Burmeister, F., W. Badowsky, T. Braun, S. Wieprich, J. Boneberg and P. Leiderer (1999). "Colloid monolayer lithography-A flexible approach for nanostructuring of surfaces." Applied Surface Science **144-145**: 461-466.

Cheng, Y., P. Jönsson and Z. Zhao (2014). Controllable fabrication of large-area 2D colloidal crystal masks with large size defect-free domains based on statistical experimental design.

Choi, J., T. L Alford and C. B Honsberg (2014). Solvent-Controlled Spin-Coating Method for Large-Scale Area Deposition of Two-Dimensional Silica Nanosphere Assembled Layers.

Choi, S. M., W. H. Kim, D. Côté, C. W. Park and H. Lee (2011). "Blood cell assisted in vivo Particle Image Velocimetry using the confocal laser scanning microscope." Optics express **19**(5): 4357-4368.

Christy, J. R. E., Y. Hamamoto and K. Sefiane (2011). "Flow Transition within an Evaporating Binary Mixture Sessile Drop." Physical Review Letters **106**(20).

Conner, J. M., et al., (1997). "Interactions between wood and distillate components in matured Scotch whisky." Flavour Science: Recent Developments.

Coomes, P. K., Barry (2019). "The Economic and Fiscal Impacts of the Distilling Industry in Kentucky."

Crampton, C. A. and L. M. Tolman (1908). "A study of the changes taking place in whiskey stored in wood." Journal of the American Chemical Society **30**(1): 98-136.

Deegan, R. D., O. Bakajin, T. F. Dupont, G. Huber, S. R. Nagel and T. A. Witten (1997). "Capillary flow as the cause of ring stains from dried liquid drops." Nature **389**(6653): 827-829.

Fan, S., M. G. Chapline, N. R. Franklin, T. W. Tombler, A. M. Cassell and H. Dai (1999). "Self-Oriented Regular Arrays of Carbon Nanotubes and Their Field Emission Properties." Science **283**(5401): 512-514.

Fullam, S., D. Cottell, H. Rensmo and D. Fitzmaurice (2000). "Carbon nanotube templated self-assembly and thermal processing of gold nanowires." Advanced materials **12**(19): 1430-1432.

Hiemenz, P. C. and R. Rajagopalan (1997). Principles of colloid and surface chemistry. New York, Marcel Dekker.

Hu, H. and R. G. Larson (2005). "Analysis of the Effects of Marangoni Stresses on the Microflow in an Evaporating Sessile Droplet." Langmuir **21**(9): 3972-3980.

Isa, L., K. Kumar, M. Müller, J. Grolig, M. Textor and E. Reimhult (2010). "Particle Lithography from Colloidal Self-Assembly at Liquid-Liquid Interfaces." ACS Nano **4**(10): 5665-5670.

J. C. Braithwaite, G. and P. F. Luckham (1997). "Effect of molecular weight on the interactions between poly(ethylene oxide) layers adsorbed to glass surfaces." Journal of the Chemical Society, Faraday Transactions **93**(7): 1409-1415.

J. Stamhuis, E. and J. Videler (1995). Quantitative Flow Analysis Around Aquatic Animals Using Laser Sheet Particle Image Velocimetry.

K, S., T. L and D. M (2003). "Experimental study of evaporating water-ethanol mixture sessile drop: influence of concentration." International Journal of Heat and Mass Transfer **46**: 4527-4534.

Karlsson, B. C. G. and R. Friedman (2017). "Dilution of whisky - the molecular perspective." Scientific Reports **7**.

Kawase, T., H. Sirringhaus, R. H. Friend and T. Shimoda (2001). "Inkjet Printed Via-Hole Interconnections and Resistors for All-Polymer Transistor Circuits." Advanced Materials **13**(21): 1601-1605.

Kendall, J. and K. P. Monroe (1917). "THE VISCOSITY OF LIQUIDS. II. THE VISCOSITY-COMPOSITION CURVE FOR IDEAL LIQUID MIXTURES.1." Journal of the American Chemical Society **39**(9): 1787-1802.

Kim, H., F. Boulogne, E. Um, I. Jacobi, E. Button and H. A. Stone (2016). "Controlled Uniform Coating from the Interplay of Marangoni Flows and Surface-Adsorbed Macromolecules." Physical Review Letters **116**(12).

Kim, M. H., S. H. Im and O. O. Park (2005). "Rapid Fabrication of Two- and Three-Dimensional Colloidal Crystal Films via Confined Convective Assembly." Advanced Functional Materials **15**(8): 1329-1335.

Li, C., G. Hong, P. Wang, D. Yu and L. Qi (2009). "Wet Chemical Approaches to Patterned Arrays of Well-Aligned ZnO Nanopillars Assisted by Monolayer Colloidal Crystals." Chemistry of Materials **21**(5): 891-897.

Liebmann, A. J. and M. Rosenblatt (1943). "Changes in Whisky while Maturing." Industrial & Engineering Chemistry **35**(9): 994-1002.

Liu, C., E. Bonaccorso and H.-J. Butt (2008). "Evaporation of sessile water/ethanol drops in a controlled environment." Physical Chemistry Chemical Physics **10**(47): 7150-7157.

Mampallil, D. and H. B. Eral (2018). "A review on suppression and utilization of the coffee-ring effect." Advances in Colloid and Interface Science **252**: 38-54.

Masuda, Y., T. Itoh and K. Koumoto (2005). "Self-Assembly Patterning of Silica Colloidal Crystals." Langmuir **21**(10): 4478-4481.

Micheletto, R., H. Fukuda and M. Ohtsu (1995). "A Simple Method for the Production of a Two-Dimensional, Ordered Array of Small Latex Particles." Langmuir **11**(9): 3333-3336.

- Nguyen, N.-T. and S. T. Wereley (2010). Fundamentals and applications of microfluidics. Boston, Mass., Artech House.
- Park, J. and J. Moon (2006). "Control of colloidal particle deposit patterns within picoliter droplets ejected by ink-jet printing." Langmuir **22**(8): 3506-3513.
- Pass, B. and I. Lambart (2003). Chapter 8 - Co-products. Whisky. I. Russell, I. Russell, C. W. Bamforth and G. G. Stewart. San Diego, Academic Press: 243-272.
- Phan, M. D., J. Lee and K. Shin (2016). "Collapsed States of Langmuir Monolayers." Journal of Oleo Science **65**(5): 385-397.
- Picknett, R. G. and R. Bexon (1977). "The evaporation of sessile or pendant drops in still air." Journal of Colloid and Interface Science **61**(2): 336-350.
- Piggott, J. R., et al. (1997). "Effect of chill filtration on whisky composition and headspace." Flavour Science: Recent Developments.
- Piggott, J. R., R. Sharp and R. E. B. Duncan (1989). The science and technology of whiskies. Harlow  
New York, Longman Scientific & Technical ;  
J. Wiley & Sons.
- Raffel, M., C. Willert and J. Kompenhans (1998). Particle Image Velocimetry: A Practical Guide.
- Rey, M., T. Yu, K. Bley, K. Landfester, D. M. A. Buzza and N. Vogel (2018). "Amphiphile-Induced Anisotropic Colloidal Self-Assembly." Langmuir **34**(34): 9990-10000.
- Ries, H. E. and H. Swift (1987). "Twisted double-layer ribbons and the mechanism for monolayer collapse." Langmuir **3**(5): 853-855.
- Ristenpart, W. D., P. G. Kim, C. Domingues, J. Wan and H. A. Stone (2007). "Influence of Substrate Conductivity on Circulation Reversal in Evaporating Drops." Physical Review Letters **99**(23): 234502.
- Sefiane, K., L. Tadrast and M. Douglas (2003). "Experimental study of evaporating water-ethanol mixture sessile drop: influence of concentration." International Journal of Heat and Mass Transfer **46**(23): 4527-4534.
- Seo, C., D. Jang, J. Chae and S. Shin (2017). "Altering the coffee-ring effect by adding a surfactant-like viscous polymer solution." Scientific Reports **7**(1): 500.
- Shedd, T. A. and A. G. Pautsch (2005). "Spray impingement cooling with single- and multiple-nozzle arrays. Part II: Visualization and empirical models." International Journal of Heat and Mass Transfer **48**(15): 3176-3184.

- Thielicke, W. (2014). "The flapping flight of birds: Analysis and application."
- Thielicke, W. a. S., E.J. (2014). "PIVlab – Towards User-friendly, Affordable and Accurate Digital Particle Image Velocimetry in MATLAB." Journal of Open Research Software.
- Varga, M. (2016). Chapter 3 - Self-assembly of nanobiomaterials. Fabrication and Self-Assembly of Nanobiomaterials. A. M. Grumezescu, William Andrew Publishing: 57-90.
- Whitesides, G. M. and B. Grzybowski (2002). "Self-Assembly at All Scales." Science **295**(5564): 2418-2421.
- Wu, Y., C. Zhang, Y. Yuan, Z. Wang, W. Shao, H. Wang and X. Xu (2013). "Fabrication of Wafer-Size Monolayer Close-Packed Colloidal Crystals via Slope Self-Assembly and Thermal Treatment." Langmuir **29**(46): 14017-14023.
- Xu, Z., L. Wang, F. Fang, Y. Fu and Z. Yin (2016). A Review on Colloidal Self-Assembly and their Applications.
- Ybert, C., W. X. Lu, G. Moller and C. M. Knobler (2002). "Collapse of a monolayer by three mechanisms." Journal of Physical Chemistry B **106**(8): 2004-2008.
- Ybert, C., W. X. Lu, G. Moller and C. M. Knobler (2002). "Kinetics of phase transitions in monolayers: collapse." Journal of Physics-Condensed Matter **14**(19): 4753-4762.
- Zhang, S., D. M. Marini, W. Hwang and S. Santoso (2002). "Design of nanostructured biological materials through self-assembly of peptides and proteins." Current Opinion in Chemical Biology **6**(6): 865-871.

## VIII. VITA

### **Martin J. Brown VI**

2452 Vale Dr.  
Lexington, KY 40514  
(859) 537-9143  
[martyjb6@gmail.com](mailto:martyjb6@gmail.com)

### **EDUCATION**

#### **University of Louisville**

Bachelor of Science, May 2018  
Major: Mechanical Engineering  
GPA: 3.82/4.00

#### **University of Louisville**

Master of Engineering, August 2019  
Major: Mechanical Engineering  
GPA: 3.96/4.00

### **WORK EXPERIENCE**

#### **University of Louisville**

*Graduate Teaching Assistant* Aug 2018 –Current

- Assisted in course covering 3D printing, PLC, Circuitry, Excel, Graphics, Python, and Engineering Ethics
- Designing new class project centered around a hydro turbine using elements above

*Undergraduate Teaching Assistant* Jan 2017 – May 2017; Aug 2015 – Dec 2015

- Tutored students in Pre-Calculus course and ENGR 101

*Student Grader* Jan 2015 – May 2016

- Responsible for creating grading rubric
- Graded Calculus I/II tests

*Outreach Team Member* Aug 2017 – May 2018

- Facilitated a weekly engineering activity at a local middle school

#### **Ford Motor Company**

Aug 2016 – Aug 2017

*SUV Paint Cooperative Internships* Louisville, KY

- Re-programmed Dürr paint robots to save 45% on paint costs and 15-20 seconds/part mule
- Created a hyperlinked embedded layout identifying plant assets using AutoCAD
- Reduced time to find spare repair parts through the improved layout

#### **Gulfstream Aerospace Corporation**

Jan 2016 – May 2016

*PP/ECS/Fuel Cooperative Internship* Savannah, GA

- Developed a fuel gauging excel program to trouble shoot jets exhibiting fuel imbalance alerts
- Detailed assembly feature review that had an FAA non-compliance AD
- Learned documentation procedure through updating documents with necessary revisions



## **Brown Forman Engineering Academy**

May 2016 – May 2017

*Mentor*

Louisville, KY

- Planned and led games aimed at highlighting the importance of communication and teamwork
- Mentored freshman during meetings fostering respectful dialogue discussing various topics

## **TECHNICAL PRESENTATIONS**

- **Presented** - ACS Colloids & Surface Science Symposium Poster Presentation (June 16-19<sup>th</sup>)
- APS Division of Fluid Dynamics Milton van Dyke Award (Nov 18-20<sup>th</sup>)

## **PUBLICATIONS**

- Co-first author “Multiscale self-assembly of unique web-like structures from evaporated drops of dilute American whiskeys”. (submitted)

## **PUBLIC OUTREACH**

- Alumni Law School Brandies, Barristers, & Bourbon (June 1<sup>st</sup>)
- ACCelerate Festival (April 5-7<sup>th</sup>)
- Kentucky Science Center Eat, Drink, Do (September 14<sup>th</sup>)

## **HONORS AND ACTIVITIES**

2019 Bennet M. Brigman Award – Attains objectives of the school

2019 WS Speed Award – contributed the most service to the school.

2018 JB Speed School Leader of the Year

Speed School Student Council – Vice President (18/19), Finance (17/18), VP of FSSSC (14/15)

2019 Engineering Exposition- Led a team of 50+ students hosting 450+ students K-12

Dean Search Student Group (2018)

Tau Beta Pi Engineering Honor Society – Secretary (17/18)

Sigma Chi International Fraternity – IFC chair, Assistant Risk Manager, Magister, Formal Chair

University of Louisville Women’s Basketball Practice Player (14/15)

Coordinated Guinness Book of World Records – Largest Secret Santa in one Location (2013)